520

ORNL-4806

ENDF-198

NATURAL CHROMIUM AND ^{52}Cr NEUTRON ELASTIC AND INELASTIC SCATTERING CROSS SECTIONS FROM 4.07 TO 8.56 MeV

W. E. Kinney

F. G. Perey

BLANK PAGE

Printed in the United States of America. Available from
National Technical Information Service
U.S. Department of Commerce
5285 Port Royal Road, Springfield, Virginia 22151
Price: Printed Copy $5.45; Microfiche $1.45

ORNL-4806
UC-79d
(ENDF-198)

Contract No. W-7405-eng-26

Neutron Physics Division

NATURAL CHROMIUM AND ^{52}Cr NEUTRON ELASTIC AND INELASTIC SCATTERING CROSS SECTIONS FROM 4.07 TO 8.56 MeV

W. E. Kinney and F. G. Perey

JANUARY 1974

OAK RIDGE NATIONAL LABORATORY
Oak Ridge, Tennessee 37830
operated by
UNION CARBIDE CORPORATION
for the
U.S. ATOMIC ENERGY COMMISSION

CONTENTS

NATURAL CHROMIUM AND ^{52}Cr NEUTRON ELASTIC AND INELASTIC SCATTERING CROSS SECTIONS FROM 4.07 TO 8.56 MeV

W. E. Kinney and F. G. Perey

ABSTRACT

Measured neutron elastic and inelastic scattering cross sections for natural chromium between 4.07 and 8.56 MeV and for ^{52}Cr between 6.44 and 8.56 MeV are presented and compared with the elastic differential cross sections of Holmqvist and Wiedling and with ENDF/B MAT 1121. Our elastic scattering differential cross sections are in fair agreement with those of Holmqvist and Wiedling. Our angle-integrated differential elastic scattering cross sections are systematically higher by as much as 17% than those of Holmqvist and Wiedling above 4.6 MeV, a situation similar to that found in comparing the two sets of data for other elements. The ENDF/B III MAT 1121 elastic angular distributions are found to be in poor agreement with experimental results from 4 to 8.5 MeV though the ENDF/B III MAT 1121 angle-integrated differential elastic scattering cross sections agree within experimental uncertainties with our results over this energy range. An evaporation model of inelastic scattering is found to be of questionable validity if applied to levels in the residual nucleus of excitation energy less than 6 MeV.

INTRODUCTION

The data reported here are the results of one of a series of experiments to measure neutron elastic and inelastic scattering cross sections at the ORNL Van de Graaffs. Reports in the series are listed in Reference 1. This report presents measured neutron elastic and inelastic scattering cross sections for natural chromium from 4.07 to 8.56 MeV and ^{52}Cr from 6.44 to 8.56 MeV. To assist in the evaluation of the data, the data acquisition and reduction techniques are first briefly discussed. For the purposes of discussion the data are presented in graphical form and are compared with the results of Holmqvist and Wiedling[2] and with ENDF/B III (Evaluated Neutron Data File B, Version III) MAT 1121. Tables of numerical values of the elastic scattering cross sections and cross sections for inelastic scattering to discrete levels in the residual nucleus are given in an appendix.

DATA ACQUISITION

The data were obtained with conventional time-of-flight techniques. Pulsed (2 MHz), bunched (approximately 1.5 nsec full width at half maximum, FWHM) deuterons accelerated by the ORNL Van de Graaffs interacted with deuterium in a gas cell to produce neutrons by the D(d,n)^{3}He reaction. The gas cells, of length 1 and 2 cm, were operated at pressures of approximately 1.5 atm and gave neutron energy resolutions of the order of ±60 keV.

The neutrons were scattered from a solid right circular cylindrical sample of natural chromium, 1.52 cm diameter, 2.56 height of mass 25.90 gm and placed approximately 10 cm from the gas cells when the detector angles were greater than 25 degrees. For smaller detector angles the cell-to-sample distance had to be increased to 33 cm in order to shield the detector from neutrons coming directly from the gas cells. The ^{52}Cr sample was in the form of a solid right circular cylinder made of 5 separate discs of pressed ^{52}Cr metallic powder with no binder. The overall dimensions were 1.76 cm diameter, 2.86 cm height, and the mass was 29.01 gm. The ^{52}Cr had oxidized considerably but the oxygen was accounted for as described in the results below.

The scattered neutrons were detected by 12.5 cm diameter NE-213 liquid scintillators optically coupled to XP-1040 photomultipliers. The scintillators were 2.5 cm thick. Data were taken with three detectors simultaneously. Flight paths were approximately 5 m with the detector angles ranging from 15 to 140 degrees. The gas cell neutron production was monitored by a time-of-flight system which used a 5 cm diameter by 2.5 cm thick NE-213 scintillator viewed by a 56-AVP photomultiplier placed about 4 m from the cell at an angle of 55 degrees with the incident deuteron beam.

For each event a PDP-7 computer was given the flight time of a detected recoil proton event with reference to a beam pulse signal, the pulse height of the recoil proton event, and identification of the detector. The electronic equipment for supplying this information to the computer consisted, for the most part, of standard commercial components. The electronic bias was set at approximately 700 keV neutron energy to ensure good pulse shape discrimination against gamma-rays at all energies.

The detector efficiencies were measured by (n,p) scattering from a 6 mm diameter polyethylene sample and by detecting source D(d,n)^{3}He neutrons at 0 degrees[3]. Both interactions gave results which agreed with each other and which yielded efficiency versus energy curves that compared well with calculations[4].

DATA REDUCTION

Central to the data reduction process was the use of a light pen with the PDP-7 computer oscilloscope display programs to extract peak areas from spectra. The light pen made a comparatively easy job of estimating errors in the cross section caused by extreme but possible peak shapes.

The reduction process started by normalizing a sample-out to a sample-in time-of-flight spectrum by the ratio of their monitor neutron peak areas, subtracting the sample-out spectrum, and transforming the difference spectrum into a spectrum of center-of-mass cross section versus excitation energy. This transformation allowed ready comparison of spectra taken at different angles and incident neutron energies by removing kinematic effects. It also made all single peaks have approximately the same shape and width regardless of excitation energy (in a time-of-flight spectrum, single peaks broaden with increasing flight time). A spectrum of the variance based on the counting statistics of the initial data was also computed. Figure 1 shows a typical time-of-flight spectrum and its transformed energy spectrum.

ORNL-DWG 73-7023

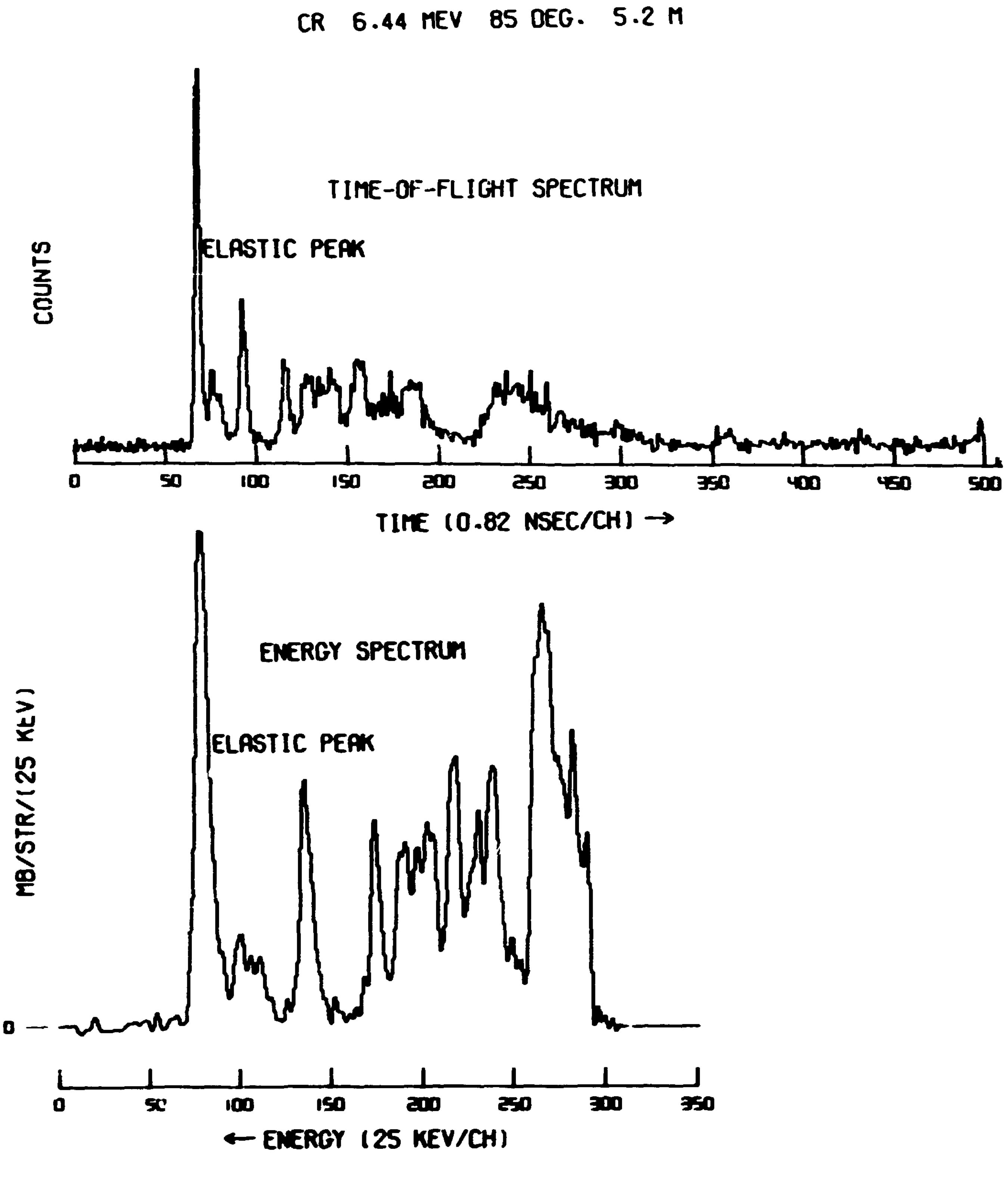

Fig. 1. A typical time-of-flight spectrum for natural chromium with its transformed energy spectrum. The data were taken at 6.44 MeV incident neutron energy at 85 degrees with a 5.2 m flight path. The sample-out spectrum has not been subtracted from the time-of-flight spectrum. Note that the energy spectrum has been offset to allow negative excursions due to statistics in the subtraction of the sample-out background. Because of uncertainties in the efficiency near the electronic bias, the energy spectrum was terminated at approximately 1 MeV scattered neutron energy - very nearly channel 350 in the time-of-flight spectrum. The large peak to the left of both spectra is the elastic peak. The small peak at roughly channel 100 of the energy spectrum is due to a 1.5% oxygen contamination of the sample.

The transformed spectra were read into the PDP-7 computer and the peak stripping was done with the aid of the light pen. A peak was stripped by drawing a background beneath it, subtracting the background, and calculating the area, centroid, and FWHM of the difference. The variance spectrum was used to compute a counting statistics variance corresponding to the stripped peak. Peak stripping errors due to uncertainties in the residual background under the peaks or to the tails of imperfectly resolved nearby peaks could be included with the other errors by stripping the peaks several times corresponding to high, low, and best estimates of this background. Although somewhat subjective, the low and high estimates of the cross sections were identified with 95% confidence limits; these, together with the best estimate, defined upper and lower errors due to stripping. When a spectrum was completely stripped, the output information was written on magnetic tape for additional processing by a large computer.

Finite sample corrections were performed according to semianalytic recipes whose constants were obtained from fits to Monte Carlo results[5]. The corrections were 6 - 12% at forward angles, 40 - 60% in the first minimum, and 10 - 13% on the second maximum.

The final error analysis included uncertainties in the geometrical parameters (scatterer size, gas cell-to-scatterer distance, flight paths, etc.) and uncertainties in the finite sample corrections.

The measured differential elastic scattering cross sections were fitted by least squares to a Legendre series:

$$\sigma(\mu = \cos\theta) = \Sigma[(2k+1)/2)]a_k P_k(\mu)$$

the points being weighted by the inverse of their variances which were computed by squaring the average of the upper and lower uncertainties. The common 7% uncertainty in absolute normalization was not included in the variances for the fitting. In order to prevent the fit from giving totally unrealistic values outside the angular range of our measurements, we resorted to the inelegant but workable process of adding three points equally spaced in angle between the largest angle of measurement and 175 degrees. The differential cross sections at the added points were chosen to approximate the diffraction pattern at large angles, but were assigned 50% errors.

RESULTS

Additional Scattering Sample Properties

Natural chromium contains 4 isotopes with natural abundances[6] 4.31% ^{50}Cr, 83.76% ^{52}Cr, 9.55% ^{53}Cr, and 2.38% ^{54}Cr. Inelastic scattering to the 1.53 MeV level in ^{53}Cr and possibly to the 1.28 MeV level in ^{53}Cr is included in our cross sections per atom of natural chromium for inelastic scattering to the 1.434 MeV level in ^{52}Cr. Similarly, inelastic scattering to the 2.23, 2.32, and 2.45 MeV levels in ^{53}Cr is included in our cross sections per atom of natural chromium for inelastic scattering to the 2.369 MeV level in ^{52}Cr. The natural chromium sample had a 1.5% oxygen contamination.

The ^{52}Cr sample had oxidized sufficiently so that oxygen elastic scattering and inelastic scattering to the 6.052 and 6.131 MeV levels in oxygen were evident in the spectra. Kinematics separated the oxygen elastic scattering from that of the ^{52}Cr at angles larger than 60 deg. and was used with our oxygen data[1] to determine the amount of oxygen in the sample to be 0.42 gm/cm^3 as opposed to a ^{52}Cr density of 3.73 gm/cm^3. The elastic scattering at smaller angles where there was no separation was thus able to be corrected for the oxygen. The oxygen inelastic scattering was sufficiently prominent and sharp so that it could be stripped from the data.

Elastic Scattering Differential Cross Sections
Natural Chromium

Our differential elastic scattering cross sections for natural chromium are shown in Figure 2 with Legendre least squares fits to the data. Wick's Limit is shown and was used as an additional point in the fittings.

Figures 3 and 4 compare our differential elastic scattering cross sections with those of Holmqvist and Wiedling (H+W)[2]. The angular distributions of ENDF/B III MAT 1121 normalized to the integrals of the experimental differential elastic scattering cross sections are also shown in the figures. The two sets of experimental data appear to be consistent so far as shapes are concerned with the first minimum falling at the same angle in both sets and slowly moving toward smaller angles with increasing energy.

The ENDF/B III MAT 1121 angular distributions are perhaps in the poorest agreement we have seen in our comparisons of our data and the data of others with ENDF/B (see Ref. 1). Previous comparisons generally agree within experimental uncertainties at angles less than 40 deg. An underestimate of the forward scattering could be a serious deficiency in the calculation of a fast reactor shield. ENDF/B III MAT 1121 uses a Legendre expansion of order 16 to describe its elastic angular distributions from 2.35 to 14 MeV while the maximum order required by the experimental data is 9.

The degree of agreement among our elastic differential cross sections and those of Holmqvist and Wiedling might be estimated with the help of Figures 5 and 6 where normalized (the coefficient of $P_0 = 1$) Legendre expansion coefficients resulting from fits to both sets of data are plotted as a function of incident neutron energy. The curves are quadratic least squares fits to our set of data with the resulting constants given in the equations. With the exception of the data at 8.05 MeV, all of the first four coefficients resulting from fits to the data of Holmqvist and Wiedling lie within the fitting uncertainties of the curves fitting our coefficients. The coefficients of the higher order polynomials are not in such good agreement, however. On this basis, then, the two sets of data can only be said to be in fair agreement.

^{52}Cr

Our ^{52}Cr differential elastic scattering cross sections are shown in Figure 7 with Legendre least squares fits and Wick's Limit which was used as an additional point in the fitting.

Our natural chromium and ^{52}Cr differential elastic scattering cross sections are compared in Figure 8 where it can be seen they agree generally well within the experimental uncertainties.

ORNL-DWG 73-7031

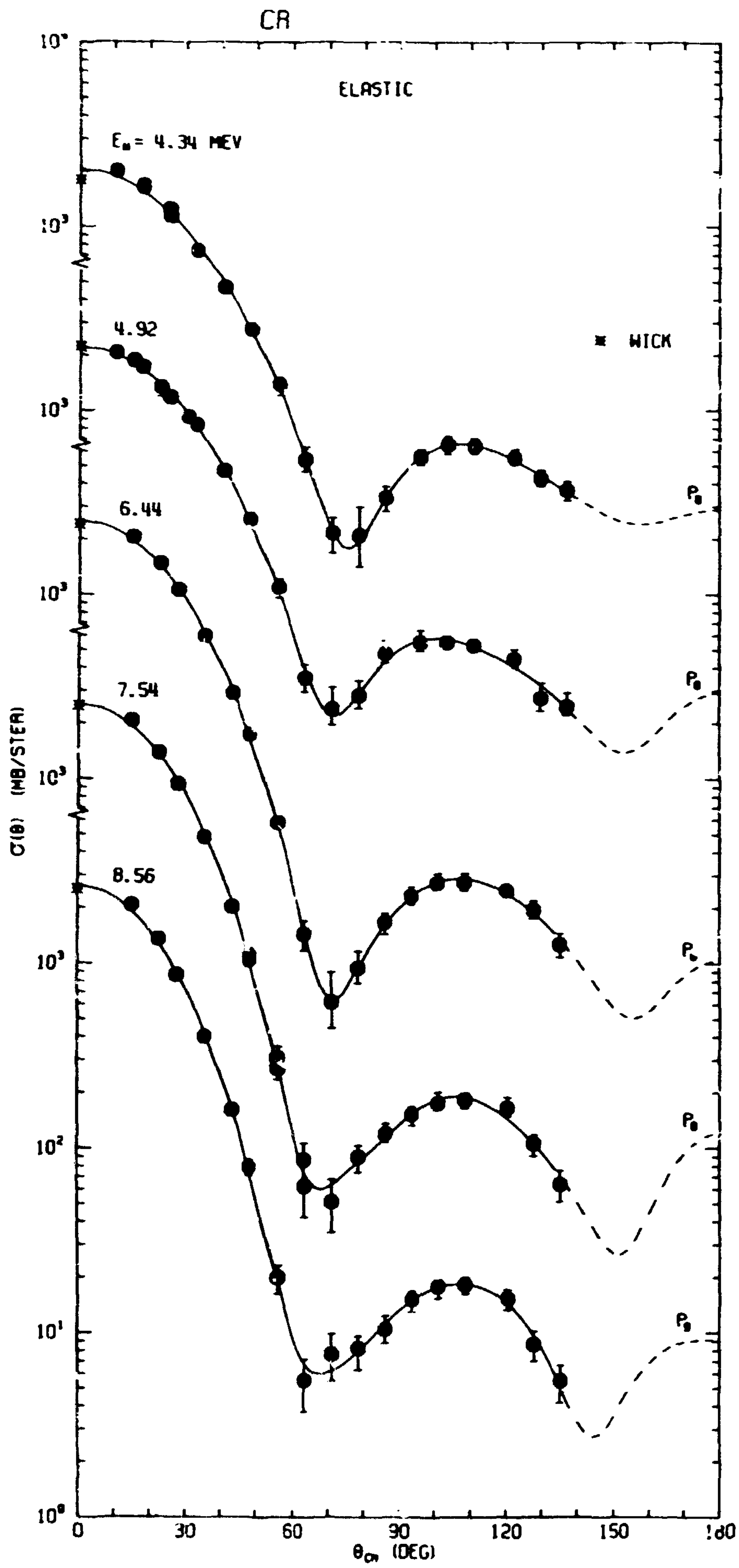

Fig. 2. Our natural chromium neutron differential elastic cross sections with Legendre fits to the data. WICK indicates Wick's Limit which was used in the fitting. The 7% uncertainty in absolute normalization common to all points is not included in the error bars.

ORNL-DWG 73-7037

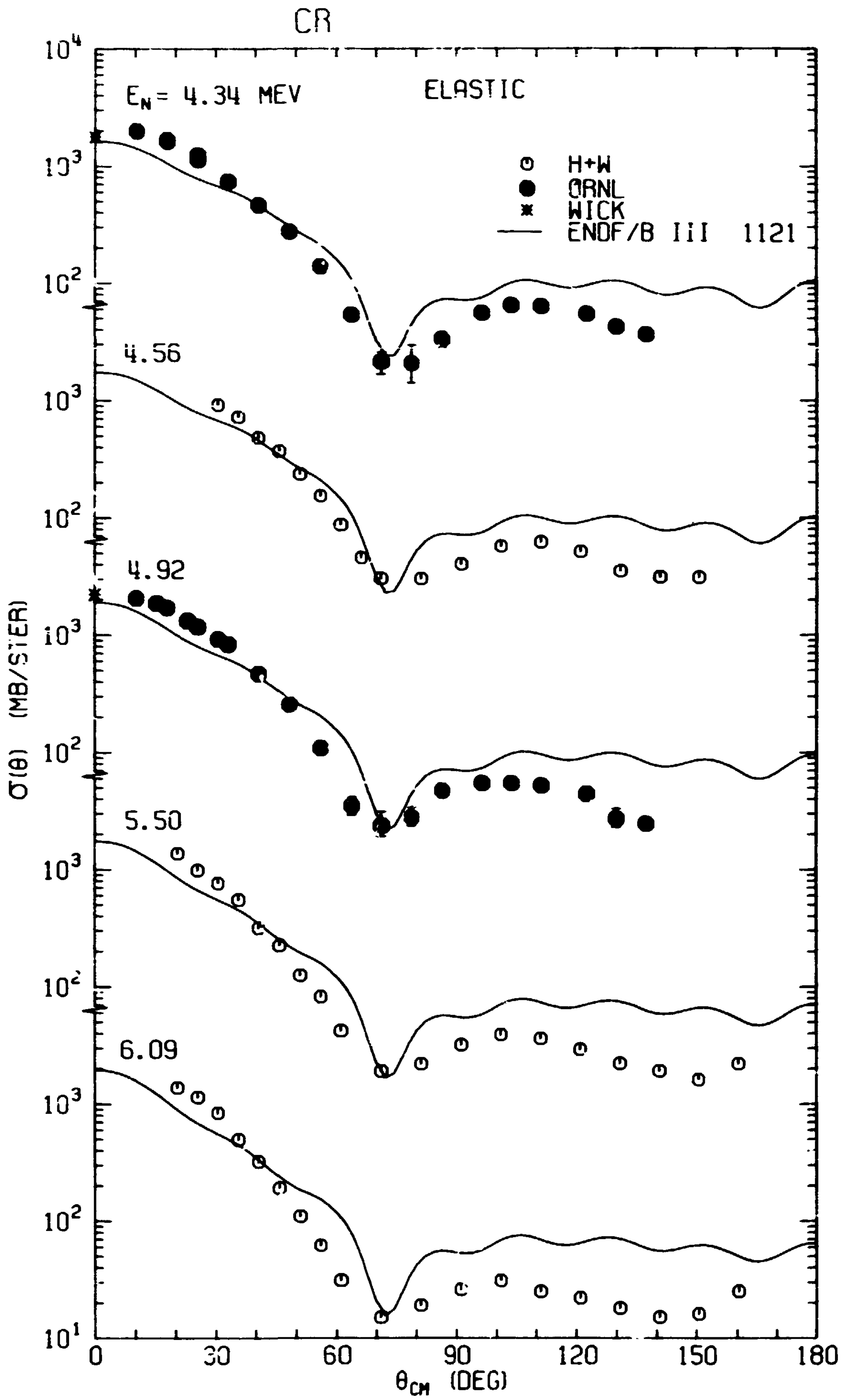

Fig. 3. Our natural chromium neutron differential elastic cross sections compared with the data of Holmqvist and Wiedling (H+W)[2] and with the angular distributions of ENDF/B III MAT 1121 from 4.34 to 6.09 MeV. WICK indicates Wick's Limit. The 7% uncertainty in absolute normalization common to all points is not included in our error bars.

ORNL-DWG 73-7035

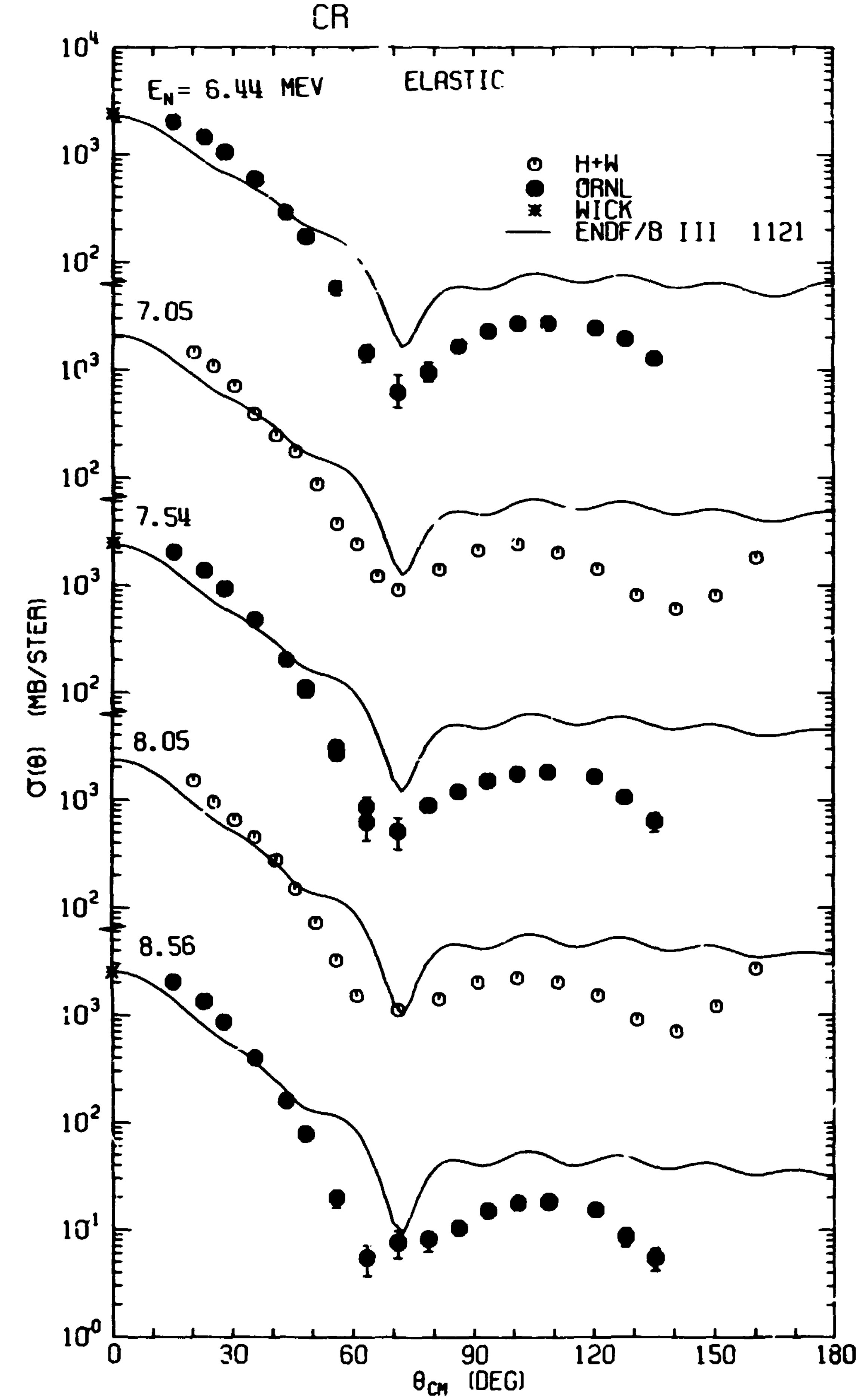

Fig. 4. Our natural chromium neutron differential elastic cross sections compared with the data of Holmqvist and Wiedling (H+W)[2] and with the angular distributions of ENDF/B III MAT 1121 from 6.44 to 8.56 MeV. WICK indicates Wick's Limit. The 7% uncertainty in absolute normalization common to all points is not included in our error bars.

ORNL-DWG 73-7024

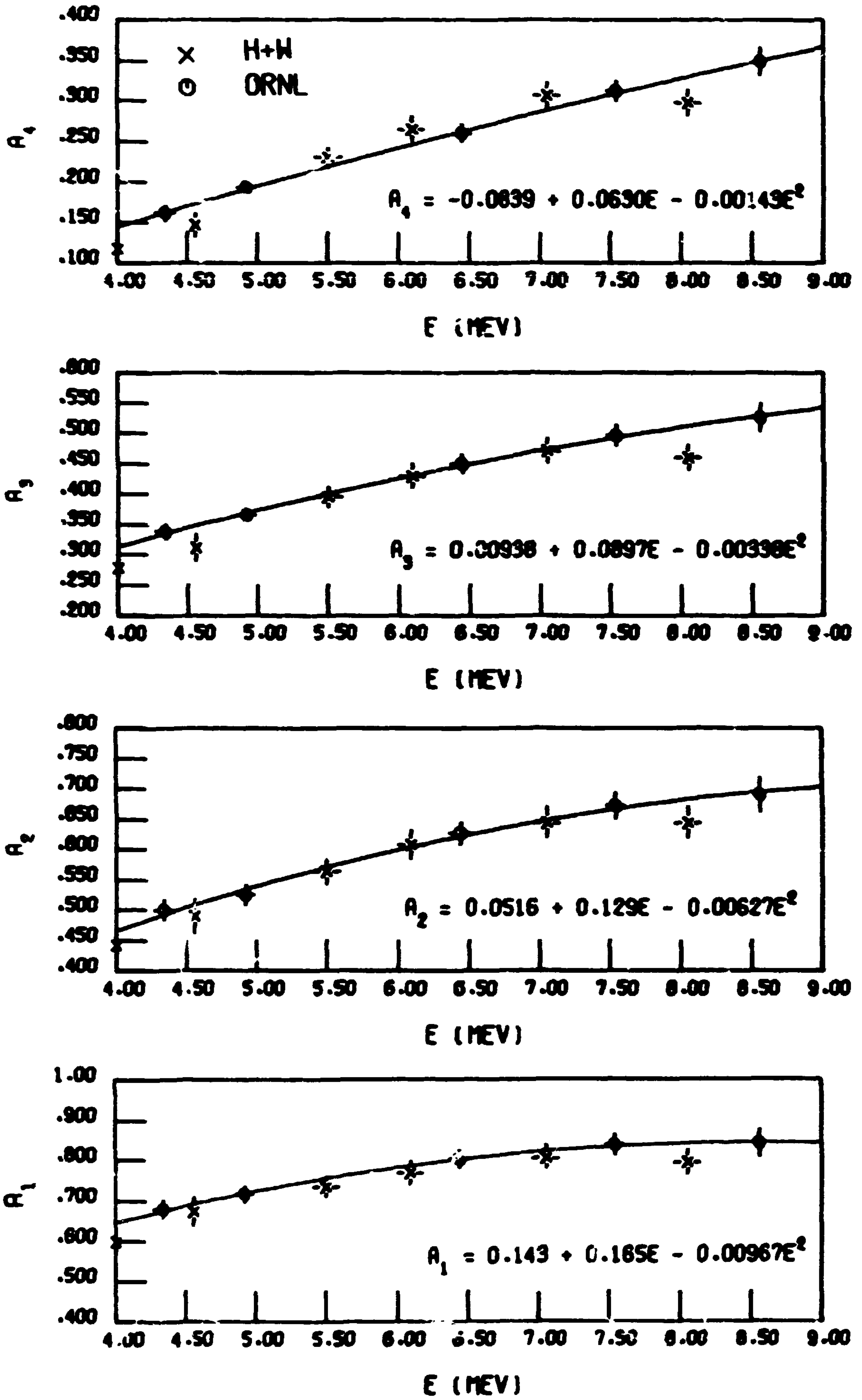

Fig. 5. The first through fourth normalized Legendre expansion coefficients obtained by fitting the natural chromium differential elastic scattering cross sections of Holmqvist and Wiedling[2] and our data as a function of incident neutron energy, E. The curves result from quadratic least squares fits to our data with constants given in the equations.

ORNL-DWG 73-7025

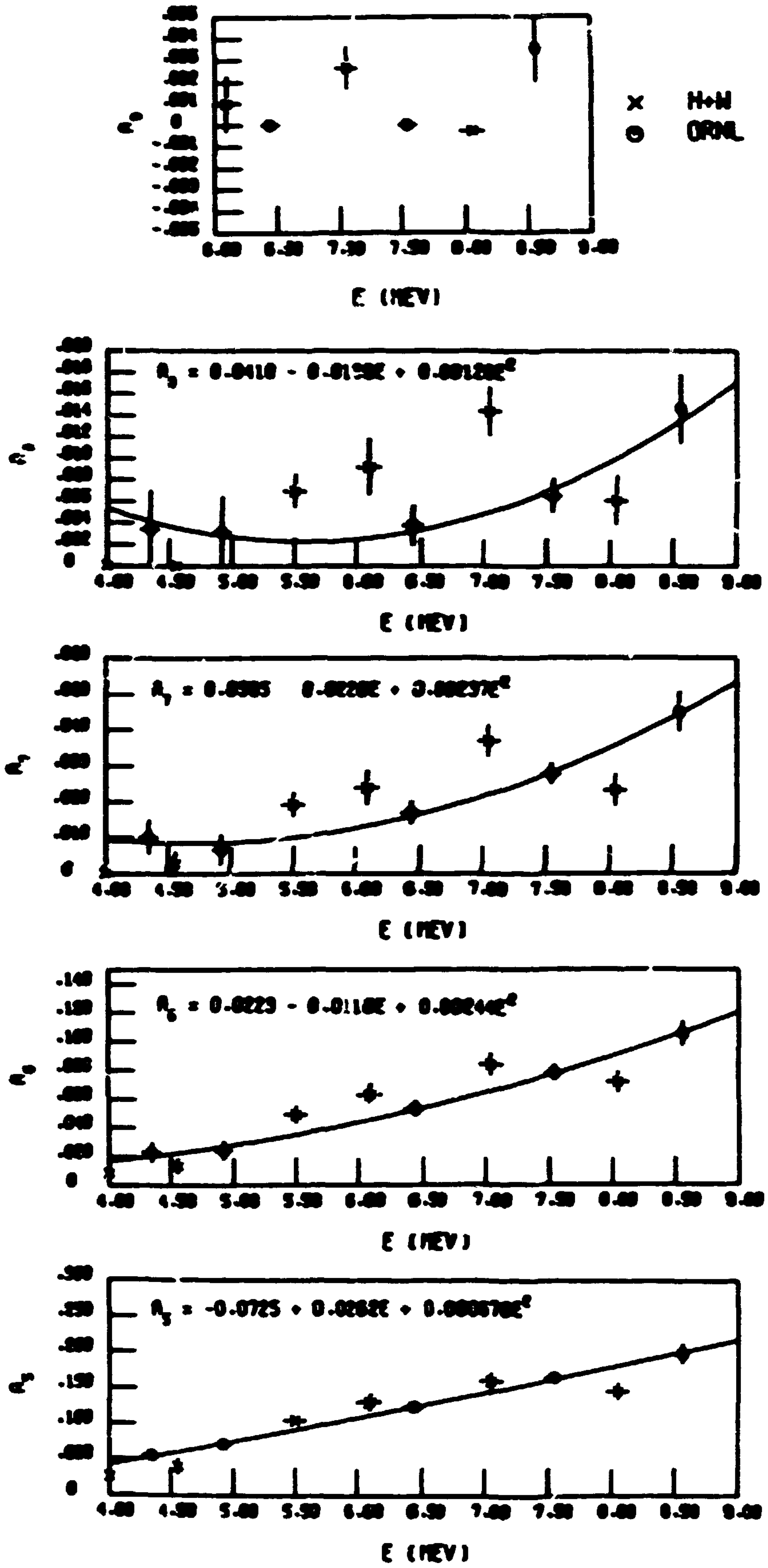

Fig. 6 The fifth through ninth normalized Legendre expansion coefficients obtained by fitting the natural chromium differential neutron elastic scattering cross sections of Holmqvist and Wiedling[2] and our data as a function of incident neutron energy, E. The curves result from quadratic least squares fits to our data with constants given in the equations.

ORNL-DWG 73-7034

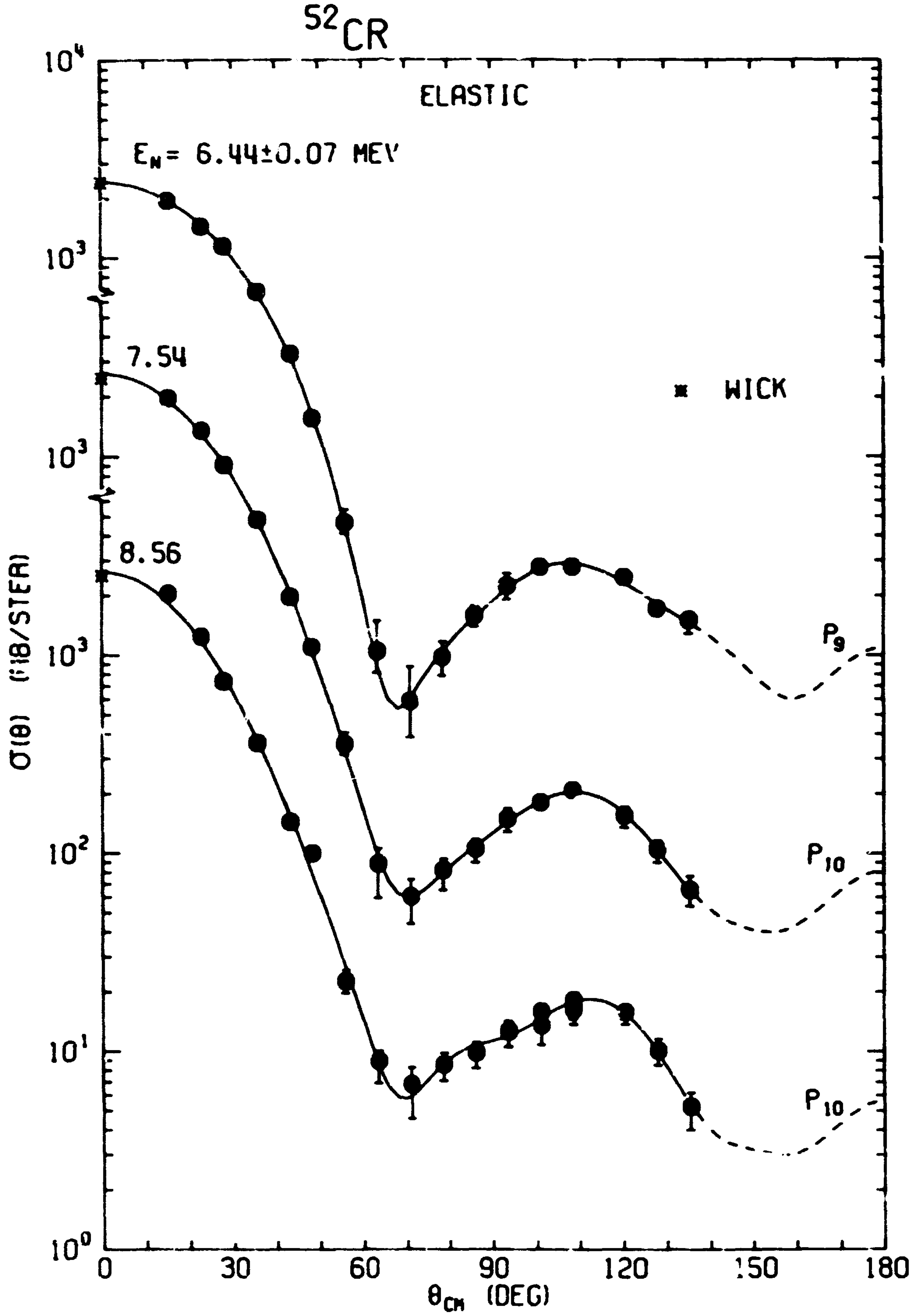

Fig. 7. Our ^{52}Cr neutron differential elastic scattering cross sections with Legendre fits to the data. WICK indicates Wick's Limit and was used in the fitting. The 7% uncertainty common to all points is not included in the error bars.

ORNL-DWG 73-7829

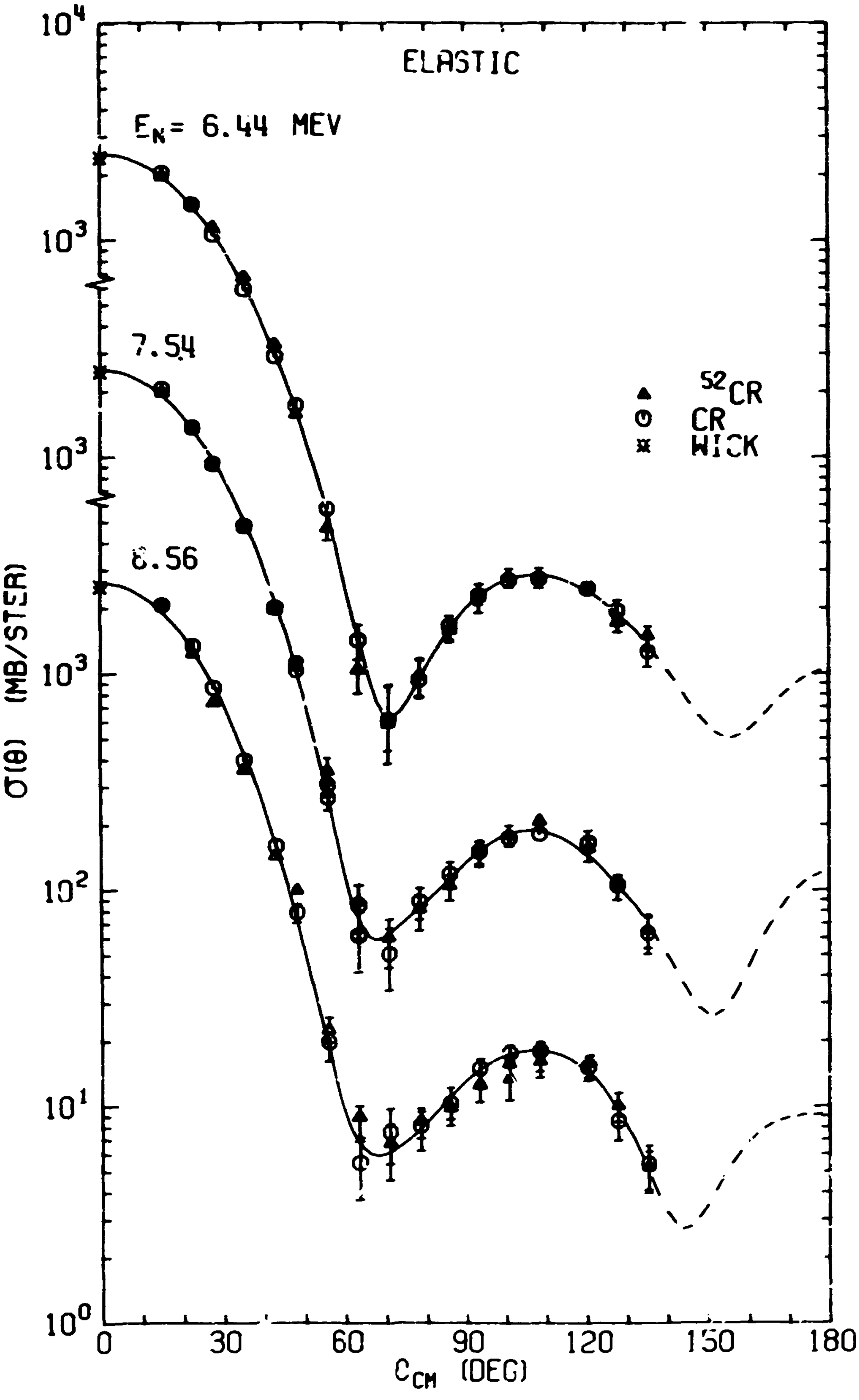

Fig. 8. A comparison of our natural chromium and ^{52}Cr neutron differential elastic scattering cross sections with Legendre least squares fits to the natural chromium data.

Inelastic Scattering Differential Cross Sections
Natural Chromium

Meaningful inelastic scattering cross sections could be obtained only for inelastic scattering to levels in ^{52}Cr for the natural chromium sample since the natural abundances of the other isotopes are so small.

Figure 9 shows our differential cross sections per atom of natural chromium for inelastic scattering to the 1.434 MeV level in ^{52}Cr. This level being a 2^{+} level, there might be some asymmetry about 90 deg. expected in the angular distribution though within the experimental uncertainties none is evident except possibly at 8.56 MeV.

Our differential cross sections per atom of natural chromium for inelastic scattering to the 2.369 MeV level in ^{52}Cr are shown in Figure 10. The angular distributions are, within experimental uncertainties, isotropic.

^{52}Cr

Our differential cross sections obtained with the ^{52}Cr sample for inelastic scattering to the 1.434 MeV level in ^{52}Cr are shown in Figure 11 where remarks similar to those above for the natural chromium sample apply.

Figure 12 shows our differential cross sections for inelastic scattering to the 2.369 MeV level in ^{52}Cr and the angular distributions, in agreement with those from the natural chromium sample, are isotropic within experimental uncertainties.

Figures 13 and 14 compare the natural chromium and ^{52}Cr differential inelastic scattering to levels in ^{52}Cr. The ^{52}Cr cross sections have been reduced by the ^{52}Cr natural isotopic abundance for the comparison. The data agree generally within experimental uncertainties.

Excitation Functions

Our angle-integrated differential cross sections per atom of natural chromium are shown as a function of energy in Figure 15. Our ^{52}Cr data are also included, the inelastic scattering cross sections having been reduced by the ^{52}Cr natural isotopic abundance. The data of Holmqvist and Wiedling[2] are shown, in addition, along with the curve from ENDF/B III MAT 1121.

Our natural chromium and ^{52}Cr data agree within experimental uncertainties and the integrated elastic data are in unusually good agreement with ENDF/B (see Ref. 1).

Although our data are in agreement with those of Holmqvist and Wiedling below 5 MeV, our data are systematically higher than theirs at higher energies, a situation similar to that encountered in comparisons made with the data of Holmqvist and Wiedling in the case of natural nickel and copper[1]. If each set of the chromium data is linearly interpolated to the energies of the other, our data are 350 mb higher at 5.50 MeV with the differences reducing roughly exponentially with increasing energy to 36 mb at 8.56 MeV. Some discussion of these systematic differences with Holmqvist and Wiedling is given in our nickel report[1].

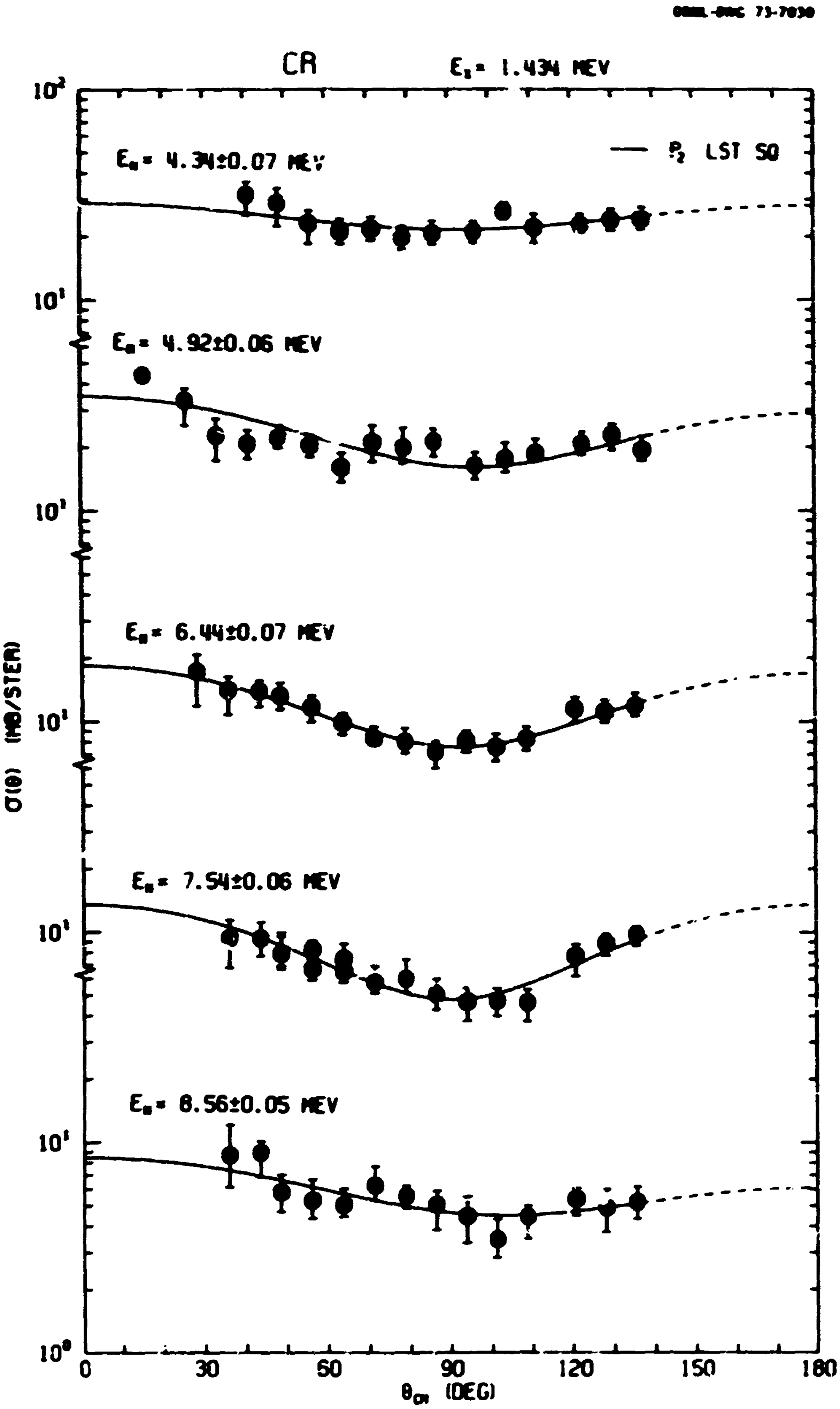

Fig. 9. Our differential cross sections per atom of natural chromium for neutron inelastic scattering to the 1.434 MeV level in ^{52}Cr. The ±7% uncertainty common to all points is not included in the error bars.

ORNL-DWG 73-7036

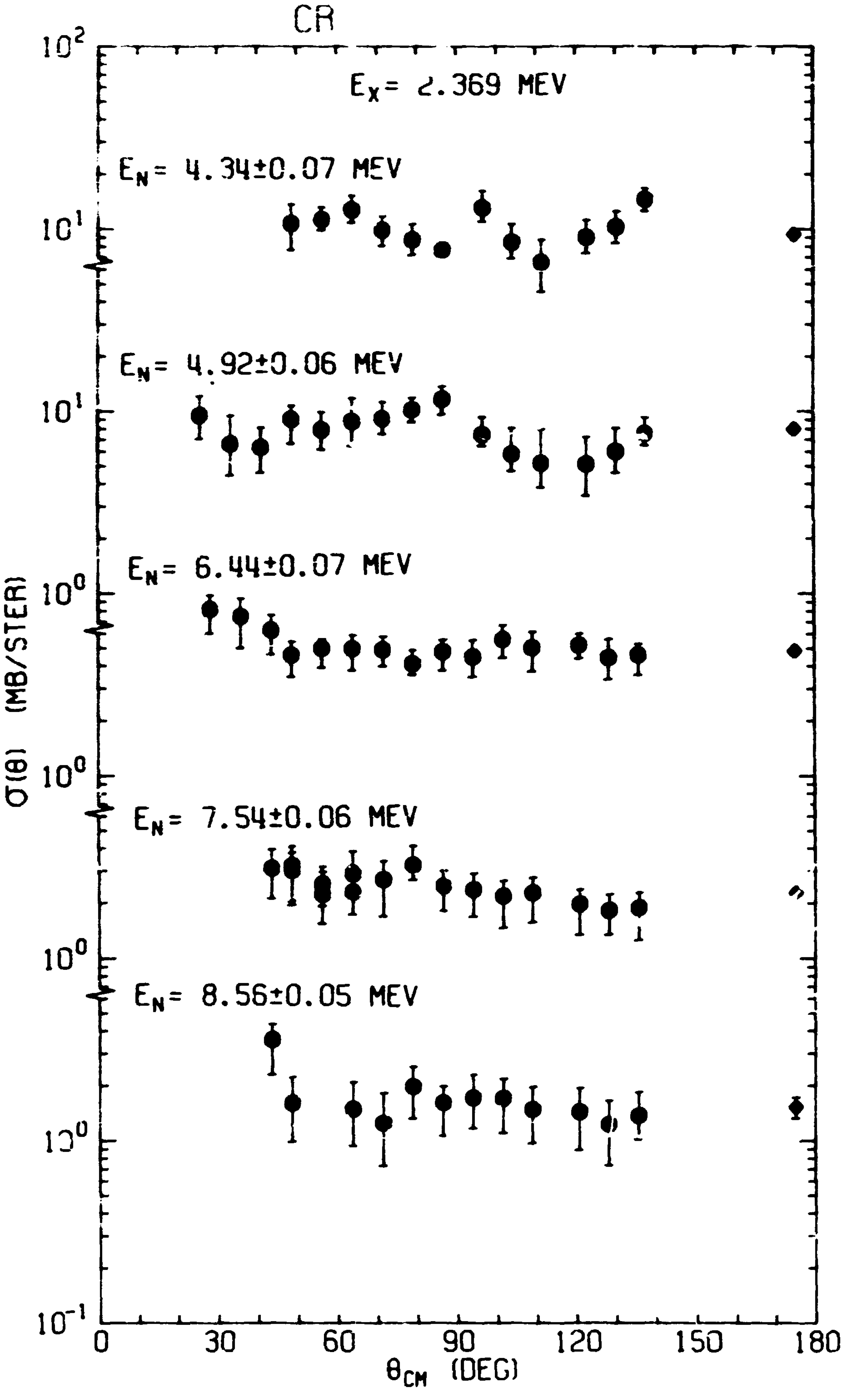

Fig. 10. Our differential cross sections per atom of natural chromium for inelastic scattering to the 2.369 MeV level in ^{52}Cr. The ±7% uncertainty common to all points is not included in the error bars.

ORNL-DWG 73-7032

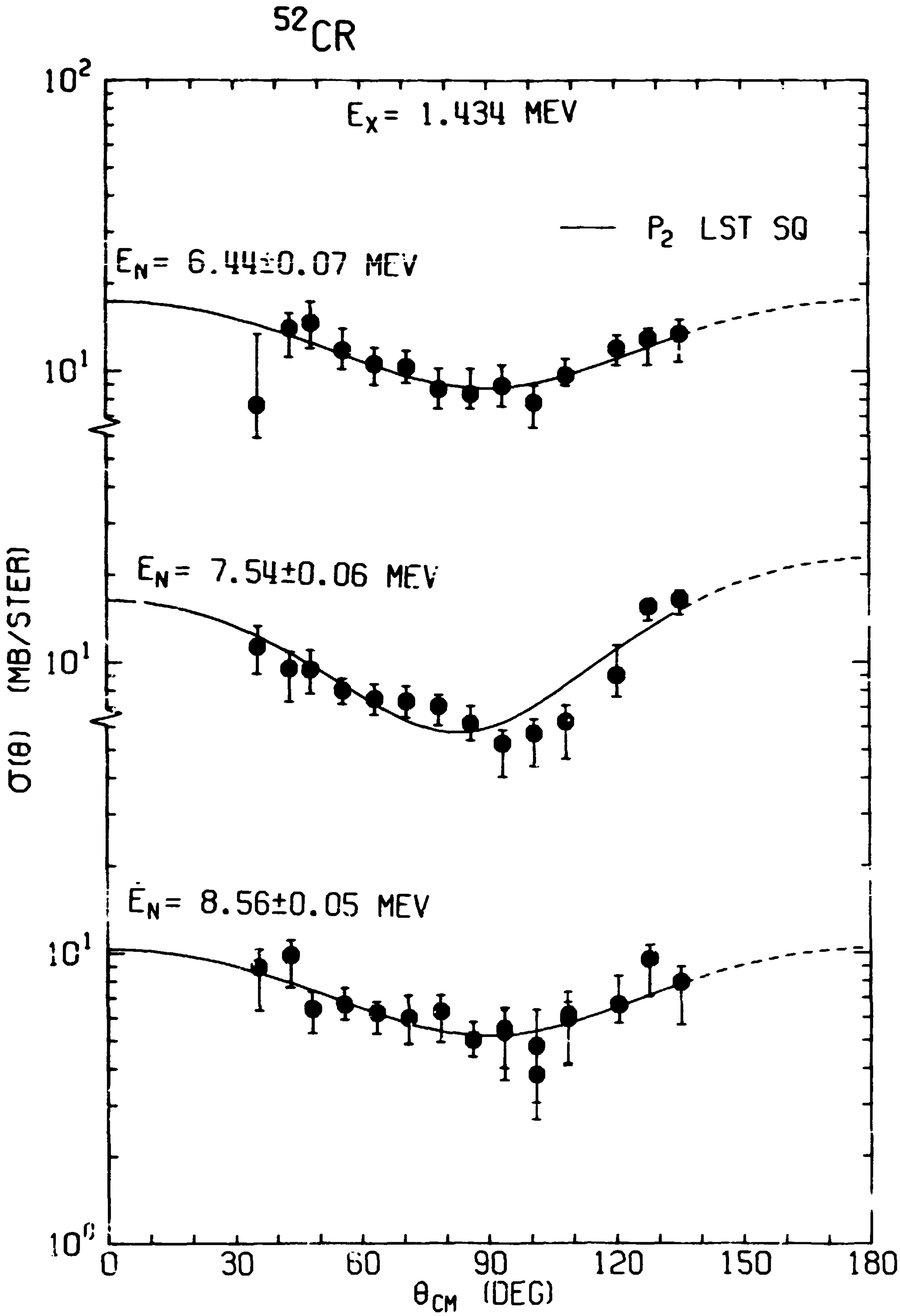

Fig. 11. Our differential cross sections for inelastic scattering to the 1.434 MeV level in ^{52}Cr as measured with the ^{52}Cr sample. The data are given per atom of ^{52}Cr. The ±7% uncertainty common to all points is not included in the error bars.

ORNL-DWG 73-7033

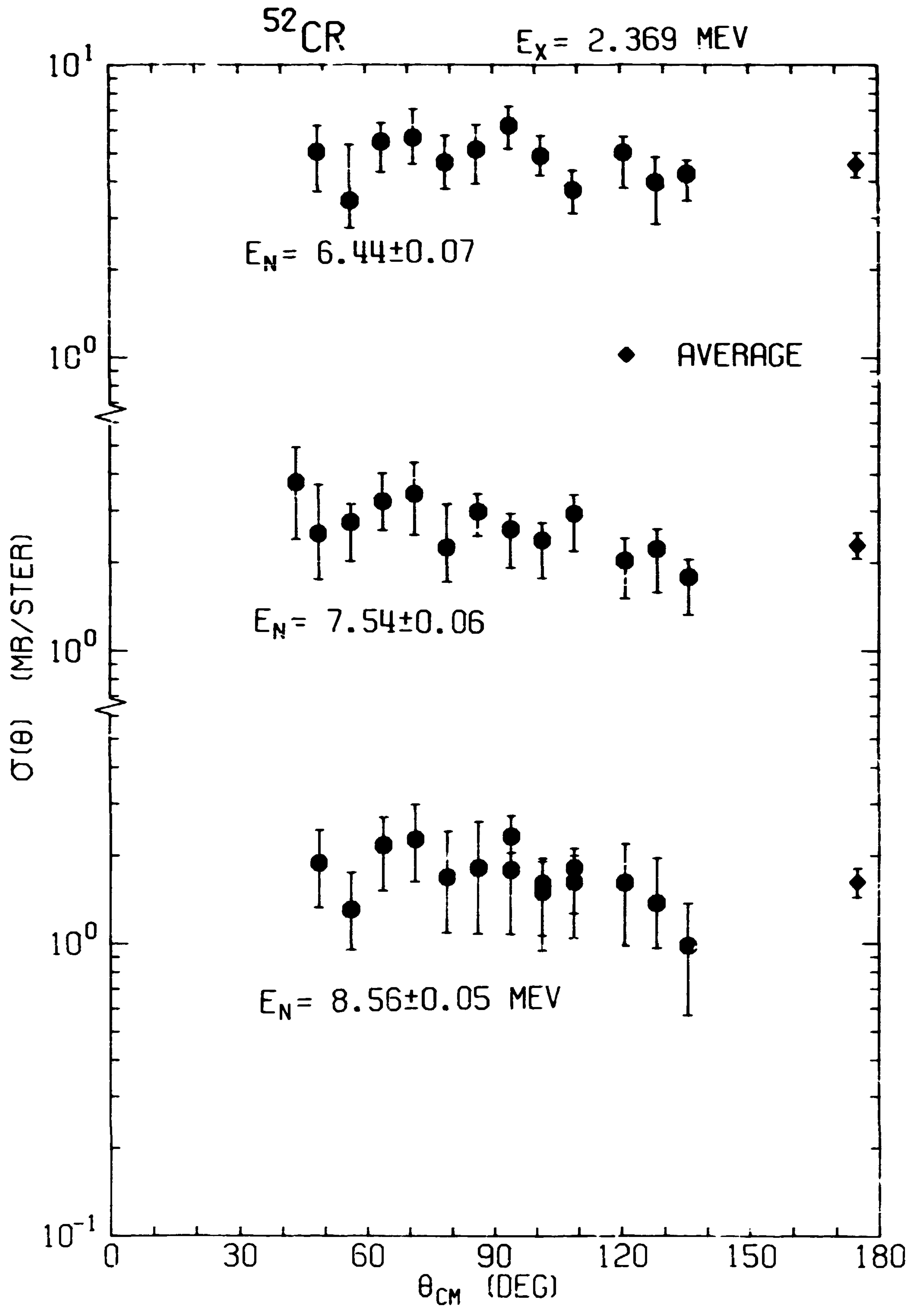

Fig. 12. Our differential cross sections for inelastic scattering to the 2.369 MeV level in ^{52}Cr as measured with the ^{52}Cr sample. The data are given per atom of ^{52}Cr. The ±7% uncertainty common to all points is not included in the error bars.

ORNL-DWG 73-7027

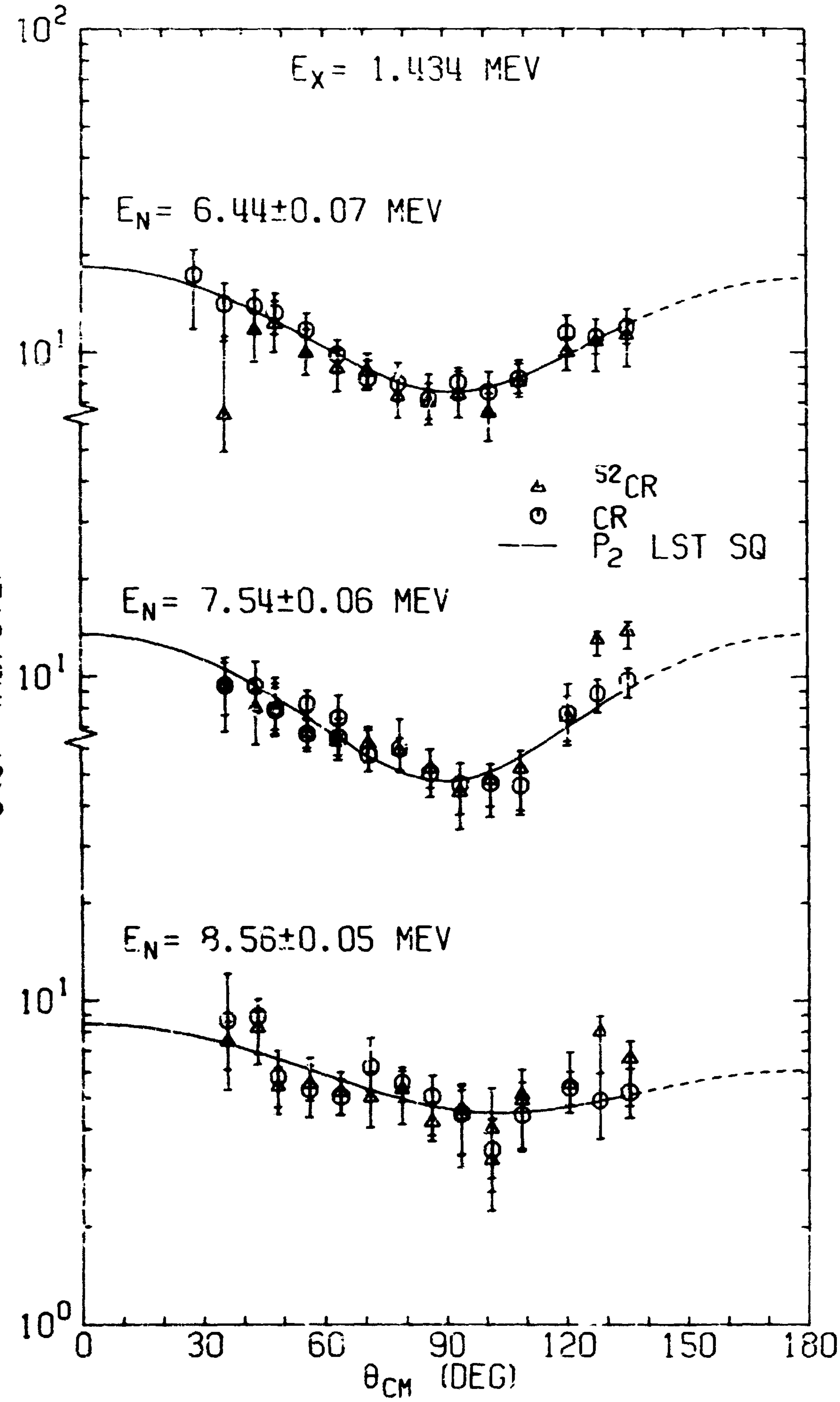

Fig. 13. A comparison of our cross sections for inelastic scattering to the 1.434 MeV level in ^{52}Cr measured with the natural chromium and the ^{52}Cr samples. The cross sections are given per atom of natural chromium. The curves are Legendre least squares fits to the natural chromium data.

ORNL-DWG 73-7028

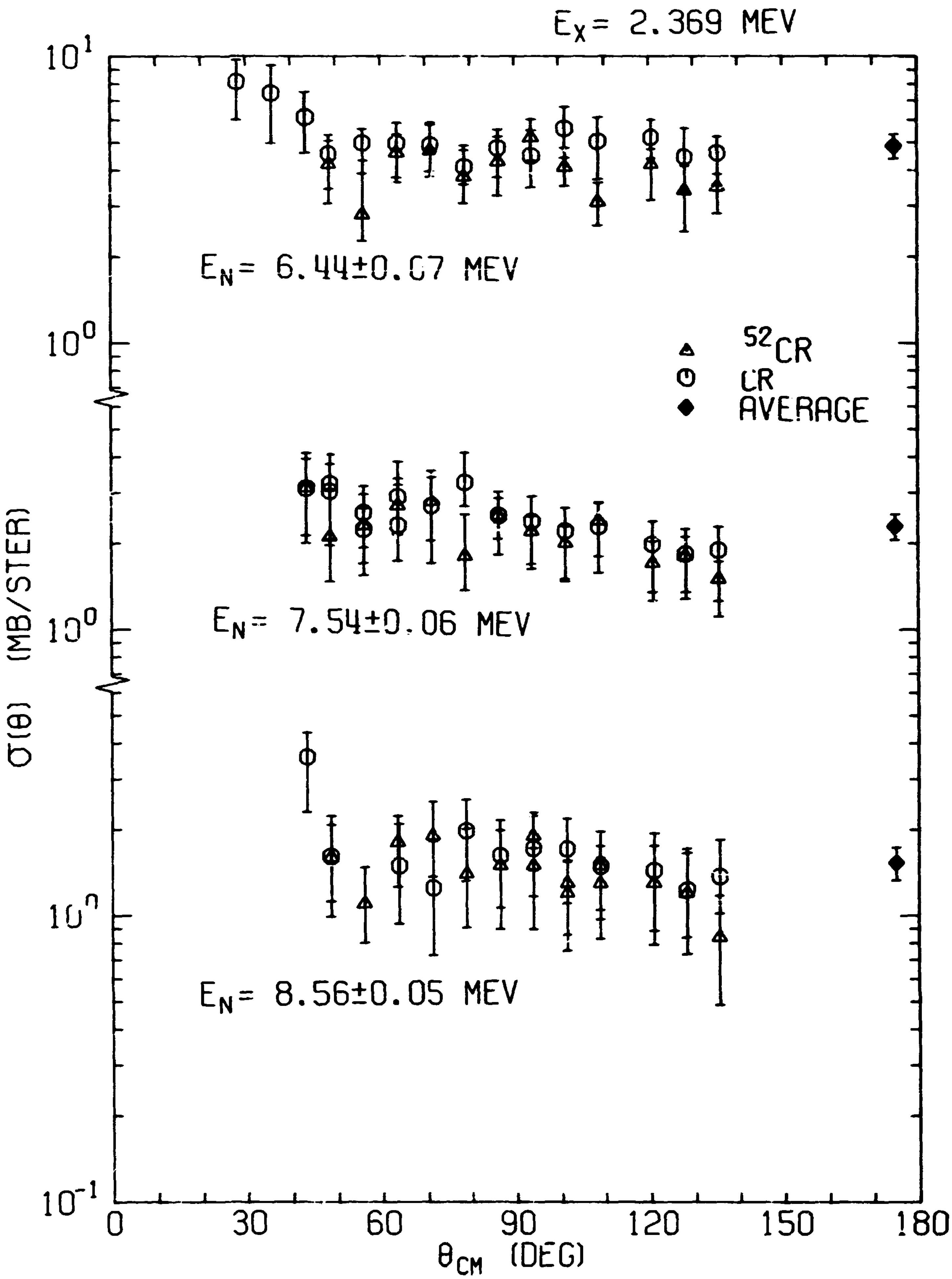

Fig. 14. A comparison of our cross sections for inelastic scattering to the 2.369 MeV level in ^{52}Cr measured with the natural chromium and the ^{52}Cr samples. The cross sections are given per atom of natural chromium.

ORNL-DWG 73-7026

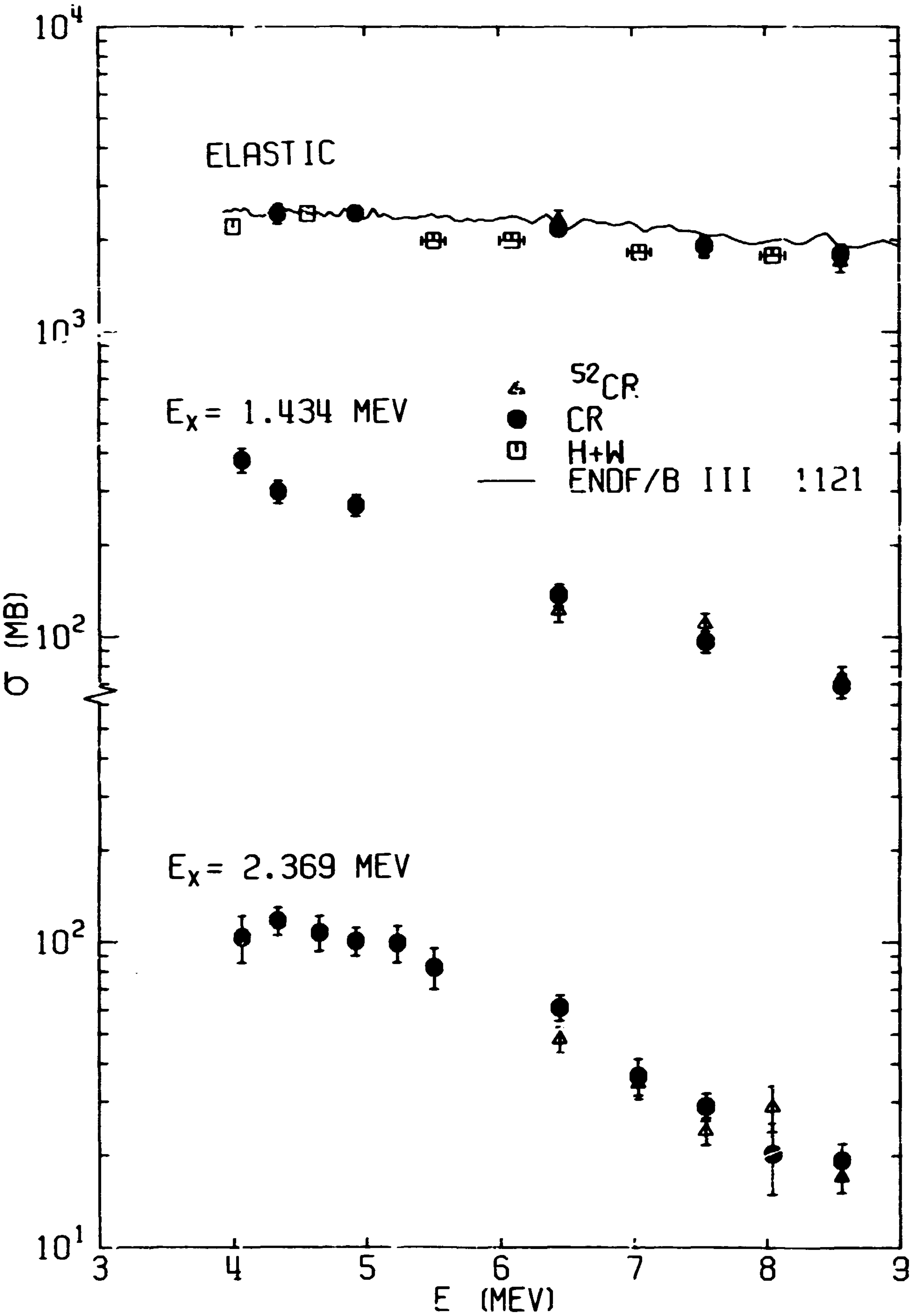

Fig. 15. Our angle-integrated cross sections for neutron elastic scattering on natural chromium and cross sections per atom of natural chromium for combined inelastic scattering to the 1.434 MeV level and the 2.369 MeV level in ^{52}Cr as a function of incident neutron energy. Elastic data of Holmqvist and Wiedling (H+W) are shown. The curves are cross sections from ENDF/B III MAT 1121.

Our natural chromium and ^{52}Cr inelastic scattering data agree within experimental uncertainties. ENDF B III MAT 1121 stops inelastic scattering to discrete levels at an incident neutron energy of 3.31 MeV, using an evaporation model with a constant nuclear "temperature" of 1 MeV to describe inelastic scattering above this incident neutron energy.

Inelastic Scattering To The Continuum

The rapidly increasing density of levels in the isotopes of natural chromium above an excitation energy of 2.369 MeV produced inelastically scattered neutron spectra, isotropic in their angular distributions, which we reduced as inelastic scattering to a structured "continuum" of final states rather than attempting to extract cross sections for inelastic scattering to groups of levels or to bands of excitation energy. Figure 16 shows our "continuum" inelastic scattering data where our angle-averaged double-differential cross sections for scattering to an excitation energy are plotted as a function of the excitation energy for all our energies of measurement. The preferential excitation of 0^+, 2^+, 4^+, 6^+, or 3^- levels at energies of 2.77, 2.96, 3.1, 3.45, 3.77, 4.1, 4.6, 5.6, and 6 MeV are clearly seen. But also there are other levels or groups of levels which were excited to produce the other structure which is evident.

The adequacy of an evaporation model in describing our inelastic "continua" may be judged from Figure 17 where SIG(E $\rightarrow$ E')/E' versus E' is plotted where SIG(E $\rightarrow$ E') = the angle-averaged differential cross section for scattering from incident energy E to exit c.m. energy dE' about E'. The straight lines are least squares fits to the data with temperatures resulting from the fits being indicated. The uncertainties on the temperatures are uncertainties in the fitting only. Two fits have been made to each set of data: one covering nearly the entire range of E' for which we extracted data and the other to an E' below which an evporation model might be more appropriate. The values of E' to which the fits were made are indicated. The fits over the entire range of E' would seem to offer a poor description of the data with there being differences of a factor of 2 among the data and the cross sections given by an evaporation model. Fits over more limited ranges in E' not surprisingly offer a better description of that data to which they are fitted as structure becomes less pronounced with increasing excitation energy (decreasing exit energy E'). As mentioned above, ENDF/B III MAT 1121 describes all inelastic scattering above incident neutron energies of 3.31 MeV by an evaporation model with a constant temperature of 1 MeV.

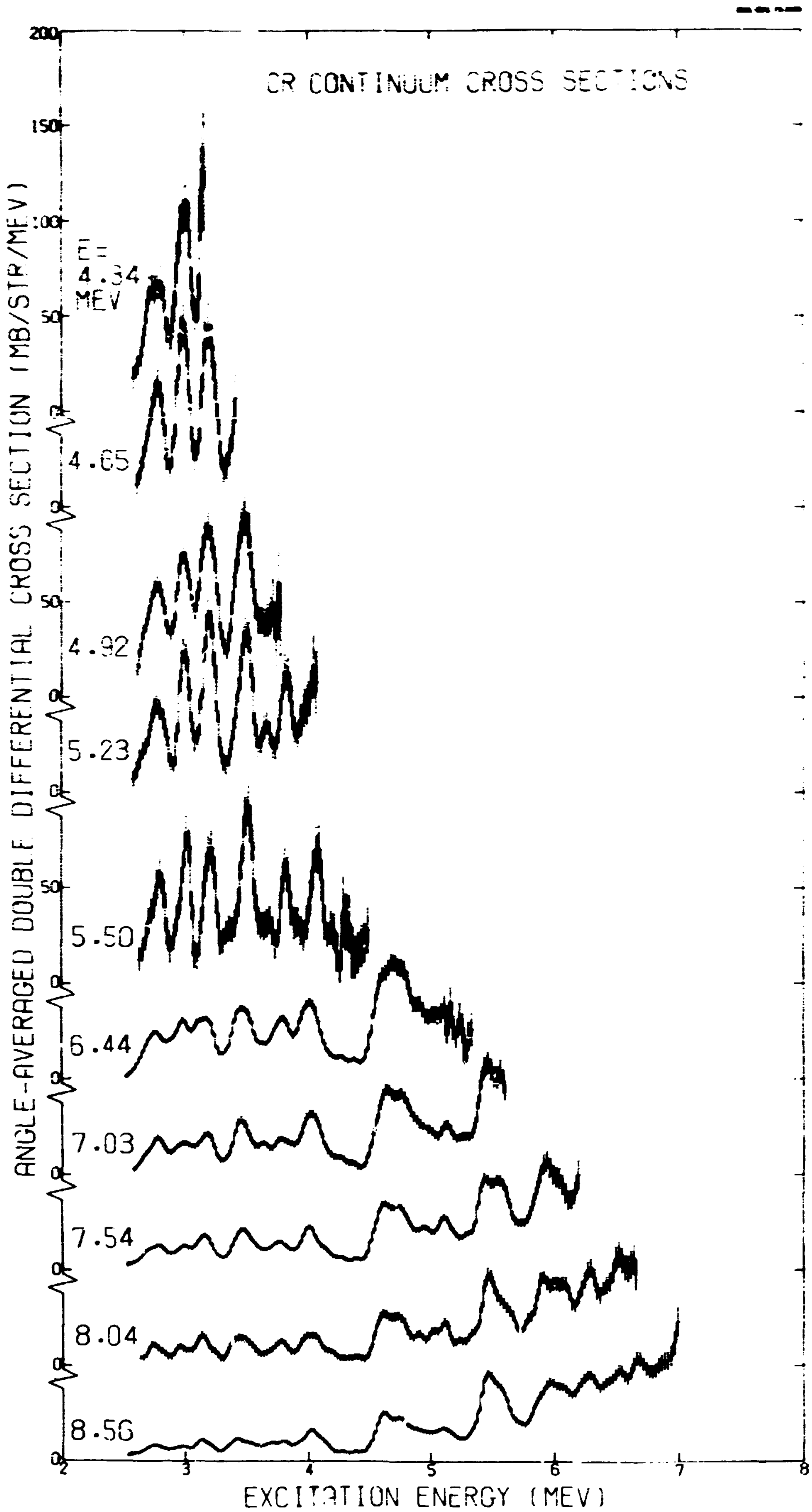

Fig. 16. Our natural chromium angle-averaged cross sections for inelastic scattering to the "continuum" as a function of excitation energy for incident neutron energies, E, from 4.34 to 8.56 MeV.

ORNL-DWG 73-7038

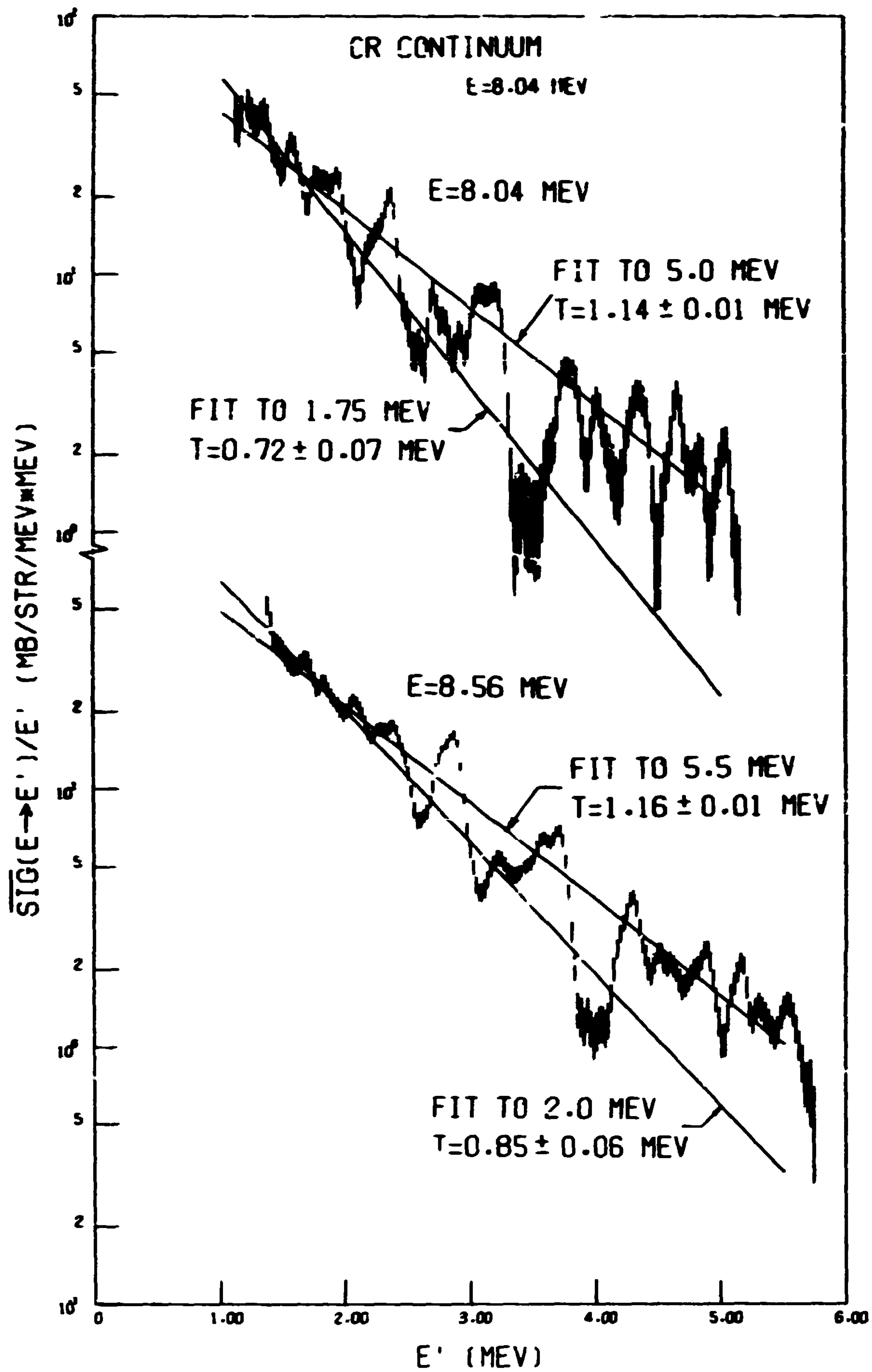

Fig. 17. Our natural chromium angle-averaged cross sections for inelastic scattering to the continuum divided by the out-going neutron energy, E', as a function of out-going neutron energy for incident neutron energies, E, from 7.54 to 8.56 MeV. Least squares fits were made to two different indicated upper limits in E' for each set of data with resulting temperatures, T, being shown. The lower value of E' was equal to the lowest value of the data in all cases.

CONCLUSIONS

Our natural chromium differential elastic scattering cross sections are in fair agreement with the data of Holmqvist and Wiedling when Legendre expansion coefficients are compared. The systematic difference in angle-integrated differential elastic cross sections above 5 MeV seen in comparisons of the two sets of data for other elements is also seen here.

The ENDF/B III MAT 1121 elastic angular distributions are in poor agreement with experimental data and underestimate the forward peak. The ENDF B III MAT 1121 angle-integrated differential elastic scattering cross sections, however, agree with our data within experimental uncertainties.

An evaporation model of inelastic scattering to levels of excitation energy in the residual nucleus greater than 6 MeV appears to offer a fair description of inelastic scattering to these levels but becomes questionable in its representation of inelastic scattering to levels of lower excitation energy.

ACKNOWLEDGMENTS

Many have contributed to this experimental program at one time or another and we would like to thank them for their contributions. In particular, we would like to acknowledge the help of J. K. Dickens, J. W. McConnell, J. A. Biggerstaff, A. M. Marusak, P. H. Stelson, C. O. LeRigoleur, and E. Hungerford.

We are deeply indebted to F. C. Maienschein, director of the Neutron Physics Division, for his support of the experiment with the use of computers in report preparation and type setting which produced this report and the other six of our last seven reports.

REFERENCES

1. F. G. Perey and W. E. Kinney, "Carbon Neutron Elastic- and Inelastic- Scattering Cross Sections from 4.5 to 8.5 MeV", ORNL-4441 (December 1970).

F. G. Perey, C. O. LeRigoleur and W. E. Kinney, "Nickel–60 Neutron Elastic- and Inelastic- Scattering Cross Sections from 6.5 to 8.5 MeV". ORNL-4523 (April 1970).

W. E. Kinney and F. G. Perey, "Neutron Elastic- and Inelastic- Scattering Cross Sections from ^{56}Fe in the Energy Range 4.19 to 8.56 MeV", ORNL-4515 (June 1970).

F. G. Perey and W. E. Kinney, "Calcium Neutron Elastic- and Inelastic- Scattering Cross Sections from 4.0 to 8.5 MeV", ORNL-4519 (April 1970).

F. G. Perey and W. E. Kinney, "Sulfur Neutron Elastic- and Inelastic- Scattering Cross Sections from 4 to 8.5 MeV", ORNL-4539 (June 1970).

W. E. Kinney and F. G. Perey, "Neutron Elastic- and Inelastic- Scattering Cross Sections for Co in the Energy Range 4.19 to 8.56 MeV", ORNL-4549 (June 1970).

W. E. Kinney and F. G. Perey, "Neutron Elastic- and Inelastic- Scattering Cross Sections for Mg in the Energy Range 4.19 to 8.56 MeV", ORNL-4550 (June 1970).

W. E. Kinney and F. G. Perey, "Neutron Elastic- and Inelastic- Scattering Cross Sections for Si in the Energy Range 4.19 to 8.56 MeV", ORNL-4517 (July 1970).

F. G. Perey and W. E. Kinney, "Neutron Elastic- and Inelastic- Scattering Cross Sections for Na in the Energy Range of 5.4 to 8.5 MeV", ORNL-4518 (August 1970).

W. E. Kinney and F. G. Perey, "Al Neutron Elastic- and Inelastic- Scattering Cross Sections from 4.19 to 8.56 MeV", ORNL-4516 (October 1970).

F. G. Perey and W. E. Kinney, "V Neutron Elastic- and Inelastic- Scattering Cross Sections from 4.19 to 8.56 MeV". ORNL-4551 (October 1970).

F. G. Perey and W. E. Kinney. "Neutron Elastic- and Inelastic- Scattering Cross Sections for Yttrium in the Energy Range 4.19 to 8.56 MeV", ORNL-4552 (December 1970).

W. E. Kinney and F. G. Perey, "Neutron Elastic- and Inelastic- Scattering Cross Sections for Oxygen in the Energy Range 4.34 to 8.56 MeV". ORNL-4780 (April 1972).

W. E. Kinney and F. G. Perey, "W Neutron Elastic- and Inelastic- Scattering Cross Sections from 4.34 to 8.56 MeV". ORNL-4803 (May 1973).

W. E. Kinney and F. G. Perey, "Natural Titanium Neutron Elastic and Inelastic Scattering Cross Sections from 4.07 to 8.56 MeV", ORNL-4810 (October 1973)

W. E. Kinney and F. G. Perey, "Natural Nickel and ^{60}Ni Neutron Elastic and Inelastic Scattering Cross Sections from 4.07 to 8.56 MeV", ORNL-4807 (to be published)

F. G. Perey and W. E. Kinney, "Nitrogen Neutron Elastic and Inelastic Scattering Cross Sections from 4.34 to 8.56 MeV", ORNL-4805 (to be published).

W. E. Kinney and F. G. Perey, "^{54}Fe Neutron Elastic and Inelastic Scattering Cross Sections from 4.34 to 8.56 MeV", ORNL-4907 (to be published).

W. E. Kinney and F. G. Perey "^{63}Cu and ^{65}Cu Neutron Elastic and Inelastic Scattering Cross Sections from 5.50 to 8.50 MeV", ORNL-4908 (to be published).

W. E. Kinney and F. G. Perey, "^{206}Pb, ^{207}Pb, and ^{208}Pb Neutron Elastic and Inelastic Scattering Cross Sections from 5.50 to 8.50 MeV", ORNL-4909 (to be published)

2. B. Holmqvist and T. Wiedling, "Neutron Elastic Scattering Cross Sections Experimental Data and Optical Model Cross Section Calculations", AE-366, Aktiebolaget Atomenergi (1969).

3. W. E. Kinney, "Neutron Elastic and Inelastic Scattering from ^{56}Fe from 4.60 to 7.55 MeV", ORNL-TM-2052, January 1968.

4. R. E. Textor and V. V. Verbinski, "05S: A Monte Carlo Code for Calculating Pulse Height Distributions Due to Monoenergetic Neutrons Incident on Organic Scintillators", ORNL-4160 (February 1968).

5. W. E. Kinney, Nucl. Instr. and Methods *83*, 15 (1970).

6. C. Michael Lederer, Jack M. Hollander, and Isadore Perlman, "Tables of Isotopes" Sixth Edition, John Wiley & Sons, Inc. (1967).

APPENDIX

Tabulated Values of Natural Chromium and ^{52}Cr Neutron Elastic Scattering Cross Sections and Cross Sections for Inelastic Scattering To Discrete Levels

Our measured values for natural chromium and ^{52}Cr neutron elastic scattering and cross sections for inelastic scattering to discrete levels are tabulated below. The uncertainties in differential cross sections, indicated by Δ in the tables, are relative and do *not* include a ±7% uncertainty in detector efficiency which is common to all points. The ±7% uncertainty is included in the integrated and average values. The total cross sections, σ_T, are those we used in the computation of Wick's Limit and were not measured by us.

We have not included the cross sections for inelastic scattering to the continuum. They are available from the National Neutron Cross Section Center, Brookhaven National Laboratory, or from us.

No attempt was made to correct angle-integrated differential cross sections for inelastic scattering to the 1.434 MeV level in ^{52}Cr at those energies at which data were taken at just three angles because of the anisotropic angular distributions of neutrons so scattered. No integrated values are therefore given in these cases.

Natural chromium cross sections may be found on pages 28 through 37. The cross sections for ^{52}Cr may be found on pages 38 through 41.

NATURAL CHROMIUM CROSS SECTIONS

Inelastic scattering cross sections are given per atom of natural chromium for inelastic scattering to levels in ^{52}Cr.

$E_n = 4.07 \pm 0.08$ MeV
(n,n') to: 1.434 MeV Level

$\theta_{c.m.}$ deg.	$d\sigma/d\omega$ mb/str	Δ (%) +	Δ (%) −
71.31	29.80	9.1	12.9
78.86	29.77	6.0	12.2
86.38	30.89	7.8	12.2

$E_n = 4.07 \pm 0.08$ MeV
(n,n') to: 2.369 MeV Level

$\theta_{c.m.}$ deg.	$d\sigma/d\omega$ mb/str	Δ (%) +	Δ (%) −
71.64	11.88	19.5	30.1
79.20	7.17	20.4	35.8
86.74	11.31	25.6	32.0

Avg. $d\sigma/d\omega$ = 8.23 mb/str ± 17.5 %
$\int(d\sigma/d\omega)d\omega$ = 103.43 mb ± 17.5 %

$E_n = 4.34 \pm 0.07$ MeV
Elastic Scattering

$\theta_{c.m.}$ deg.	$d\sigma/d\omega$ mb/str	Δ (%) +	Δ (%) −
10.20	1999.63	6.5	8.6
17.83	1630.06	5.4	9.1
17.83	1671.67	5.7	7.1
25.47	1240.12	5.7	7.2
25.47	1131.93	4.9	5.4
33.09	737.58	5.4	11.2
40.71	463.61	5.9	8.4
48.32	273.63	6.5	5.8
55.91	137.06	8.4	12.2
63.48	53.22	16.9	13.5
71.04	21.18	20.9	21.8
78.58	20.61	42.8	32.1
86.10	33.01	15.0	15.5
96.10	55.28	9.0	9.6
103.58	64.35	10.9	10.8
111.04	63.30	9.6	8.7
122.45	54.53	10.8	7.9
129.86	42.41	10.5	9.2
137.26	36.36	11.5	11.4

$\int(d\sigma/d\omega)d\omega$ = 2440.99 mb ± 7.3 %
Wick's Limit = 1786.03 mb ± 7.3 %
σ_T = 3.74 b ± 1.0 %

Legendre Fit, Order = 8

k	a_k	Δ(%)
0	388.49658	2.0
1	263.73169	2.4
2	194.42198	2.6
3	131.38455	3.0
4	62.81519	5.3
5	21.49561	13.4
6	8.86383	28.6
7	3.90331	48.1
8	1.32871	104.2

$E_n = 4.34 \pm 0.07$ MeV
(n,n') to. 1.434 MeV Level

θ_{cm} deg.	$d\sigma/d\omega$ mb/str	Δ (%) +	Δ (%) −
40.88	31.61	14.8	20.1
48.50	28.90	16.9	22.8
56.11	23.13	14.5	20.3
63.70	21.15	14.2	12.9
71.27	21.76	13.8	11.9
78.83	19.80	12.9	12.4
86.35	20.72	13.9	11.2
96.35	21.09	11.5	11.4
103.83	26.38	9.7	8.5
111.27	22.07	15.6	15.9
122.66	22.82	11.7	8.7
130.06	24.05	12.2	11.3
137.43	24.22	13.6	11.0

$\int(d\sigma/d\omega)d\omega$ = 299.10 mb ± 8.4 %

Legendre Fit, Order = 2

k	a_k	Δ(%)
0	47.60388	4.6
1	0.27926	484.6
2	1.86223	64.4

$E_n = 4.34 \pm 0.07$ MeV
(n,n') to: 2.369 MeV Level

θ_{cm} deg.	$d\sigma/d\omega$ mb/str	Δ (%) +	Δ (%) −
48.73	10.73	27.1	28.7
56.37	11.28	15.6	12.4
63.97	12.78	19.9	15.2
71.56	9.87	18.6	18.0
79.14	8.75	21.2	17.7
86.66	7.68	10.1	10.1
96.66	13.11	23.4	16.4
104.12	8.49	25.6	18.6
111.56	6.58	32.8	31.1
122.91	9.01	23.7	18.6
130.29	10.26	21.5	18.6
137.64	14.56	14.9	14.0

Avg. $d\sigma/d\omega$ = 9.34 mb/str ± 10.3 %
$\int(d\sigma/d\omega)d\omega$ = 117.41 mb ± 10.3 %

$E_n = 4.65 \pm 0.07$ MeV
(n,n') to: 1.434 MeV Level

θ_{cm} deg.	$d\sigma/d\omega$ mb/str	Δ (%) +	Δ (%) −
71.26	18.71	13.9	15.8
78.81	14.50	18.4	16.9
86.33	15.93	14.8	9.0

$E_n = 4.65 \pm 0.07$ MeV
(n,n') to: 2.369 MeV Level

θ_{cm} deg.	$d\sigma/d\omega$ mb/str	Δ (%) +	Δ (%) −
71.50	8.76	21.6	13.5
79.06	8.75	21.8	19.2
86.59	7.37	29.7	18.6

Avg. $d\sigma/d\omega$ = 8.55 mb/str ± 13.2 %
$\int(d\sigma/d\omega)d\omega$ = 107.43 mb ± 13.2 %

$E_n = 4.65 \pm 0.07$ MeV
(n,n') to: 2.648 MeV Level
+ 2.766 MeV Level

θ_{cm} deg.	$d\sigma/d\omega$ mb/str	Δ (%) +	Δ (%) −
71.64	12.18	14.4	20.8
79.21	12.46	20.6	27.0
86.75	9.64	18.0	25.3

Avg. $d\sigma/d\omega$ = 10.73 mb/str ± 14.9 %
$\int(d\sigma/d\omega)d\omega$ = 134.82 mb ± 14.9 %

$E_n = 4.65 \pm 0.07$ MeV
(n,n') to: 2.965 MeV Level

θ_{cm} deg.	$d\sigma/d\omega$ mb/str	Δ (%) +	Δ (%) −
71.76	13.98	15.0	20.9
79.33	13.27	20.9	24.6
86.86	11.09	17.7	18.0

Avg. $d\sigma/d\omega$ = 12.21 mb/str ± 14.7 %
$\int(d\sigma/d\omega)d\omega$ = 153.41 mb ± 14.7 %

$E_n = 4.65 \pm 0.07$ MeV
(n,n') to: 3.112 MeV Level
+ 3.160 MeV Level

θ_{cm} deg.	$d\sigma/d\omega$ mb/str	Δ (%) +	Δ (%) −
71.88	13.58	15.2	20.9
79.46	14.33	23.7	25.3
87.00	12.15	18.7	22.5

Avg. $d\sigma/d\omega$ = 12.99 mb/str ± 15.2%
$\int(d\sigma/d\omega)d\omega$ = 163.29 mb ± 15.2 %

$E_n = 4.65 \pm 0.07$ MeV
(n,n') to: 3.430 MeV Level
+ 3.490 MeV Level

θ_{cm} deg.	$d\sigma/d\omega$ mb/str	Δ (%) +	Δ (%) −
72.09	15.17	17.3	28.4
79.69	16.40	14.6	24.9
87.23	12.92	21.3	23.6

Avg. $d\sigma/d\omega$ = 14.20 mb/str ± 17.5%
$\int(d\sigma/d\omega)d\omega$ = 176.50 mb ± 17.5 %

$E_n = 4.92 \pm 0.06$ MeV
Elastic Scattering

θ_{cm} deg.	$d\sigma/d\omega$ mb/str	Δ (%) +	Δ (%) −
10.20	2061.16	4.9	6.0
15.29	1865.86	5.5	7.2
17.84	1715.11	6.1	8.6
22.93	1323.17	8.2	10.2
25.47	1170.57	6.9	9.3
25.47	1176.37	5.2	5.6
30.56	918.06	6.9	6.8
33.10	830.85	6.2	8.3
40.71	465.64	5.7	6.2
48.32	254.14	5.9	5.1
55.91	107.83	10.9	11.9
63.48	34.72	18.4	15.8
71.04	23.50	31.3	17.9
78.58	27.83	20.5	14.7
86.10	47.10	17.4	10.6
96.10	54.19	16.0	10.1
103.58	54.29	9.0	8.1
111.04	52.30	10.6	6.9
122.44	44.17	12.4	9.1
129.86	27.16	20.6	14.7
137.26	24.37	18.9	9.8

$\int(d\sigma/d\omega)d\omega$ = 2444.91 mb ± 7.2 %
Wick's Limit = 2224.29 mb ± 7.3 %
σ_T = 3.92 b ± 1.0 %

Legendre Fit, Order = 8

k	a_k	Δ(%)
0	389.12012	1.8
1	278.49316	2.1
2	204.45857	2.3
3	141.91414	2.6
4	75.05717	4.2
5	27.65166	9.5
6	9.39938	23.6
7	2.54682	64.0
8	1.22824	102.1

$E_n = 4.92 \pm 0.06$ MeV
(n,n′) to: 1.434 MeV Level

θ_{cm} deg.	$d\sigma/d\omega$ mb/str	Δ (%) +	Δ (%) −
15.34	44.12	6.5	6.5
25.56	33.43	13.7	24.0
33.21	22.84	19.7	24.3
40.85	20.88	15.7	15.2
48.47	22.29	13.9	10.6
56.08	20.52	11.3	12.3
63.67	16.09	16.4	15.2
71.24	21.22	20.0	19.4
78.7[illegible]	20.03	23.8	15.9
86.31	21.37	14.5	15.4
96.31	16.43	15.2	14.3
103.79	17.71	18.7	14.1
111.24	18.80	16.3	8.1
122.63	20.91	13.2	11.8
130.03	22.99	12.3	15.6
137.41	19.47	15.7	11.2

$\int(d\sigma/d\omega)d\omega = 269.79$ mb $\pm$ 7.8 %

Legendre Fit, Order = 2

k	a_k	Δ(%)
0	42.93855	3.5
1	2.02639	45.5
2	4.19227	18.2

$E_n = 4.92 \pm 0.06$ MeV
(n,n′) to: 2.369 MeV Level

θ_{cm} deg.	$d\sigma/d\omega$ mb/str	Δ (%) +	Δ (%) −
25.66	9.50	27.5	25.8
33.33	6.58	42.9	32.8
41.00	6.31	27.9	27.7
48.64	8.99	18.7	26.6
56.27	7.89	24.9	22.4
63.88	8.78	33.9	26.9
71.45	9.12	23.1	17.9
79.01	10.17	16.4	14.2
86.54	11.68	17.1	17.8
96.55	7.46	24.2	13.9
104.01	5.84	38.9	19.4
111.46	5.20	54.0	26.6
122.83	5.13	40.4	33.3
130.21	6.02	34.0	23.9
137.57	7.57	21.8	14.1

Avg. $d\sigma/d\omega$ = 8.01 mb/str ± 10.6%
$\int(d\sigma/d\omega)d\omega$ = 100.71 mb ± 10.6 %

$E_n = 5.23 \pm 0.05$ MeV
(n,n′) to: 1.434 MeV Level

θ_{cm} deg.	$d\sigma/d\omega$ mb/str	Δ (%) +	Δ (%) −
71.22	11.43	16.9	17.9
78.77	10.16	22.6	17.5
86.30	12.02	14.5	14.0

$E_n = 5.23 \pm 0.05$ MeV
(n,n′) to: 2.369 MeV Level

θ_{cm} deg.	$d\sigma/d\omega$ mb/str	Δ (%) +	Δ (%) −
71.42	8.29	17.3	18.1
78.98	9.00	17.9	17.0
86.50	6.32	24.3	14.9

Avg. $d\sigma/d\omega$ = 7.90 mb/str ± 13.7%
$\int(d\sigma/d\omega)d\omega$ = 99.29 mb ± 13.7 %

$E_n = 5.23 \pm 0.05$ MeV
(n,n') to: 2.648 MeV Level
+ 2.766 MeV Level

θ_{cm}	$d\sigma/d\omega$	Δ (%)	
deg.	*mb/str*	+	−
71.52	9.15	17.4	19.8
79.08	9.93	15.8	29.6
86.62	8.14	17.5	22.4

Avg. $d\sigma/d\omega$ = 8.69 mb/str ± 14.4%
$\int(d\sigma/d\omega)d\omega$ = 109.23 mb ± 14.4 %

$E_n = 5.23 \pm 0.05$ MeV
(n,n') to: 2.965 MeV Level

θ_{cm}	$d\sigma/d\omega$	Δ (%)	
deg.	*mb/str*	+	−
71.60	9.62	16.5	16.1
79.17	9.45	18.5	27.0
86.70	9.36	19.3	25.5

Avg. $d\sigma/d\omega$ = 9.50 mb/str ± 13.3%
$\int(d\sigma/d\omega)d\omega$ = 119.32 mb ± 13.3 %

$E_n = 5.23 \pm 0.05$ MeV
(n,n') to: 3.112 MeV Level
+ 3.160 MeV Level

θ_{cm}	$d\sigma/d\omega$	Δ (%)	
deg.	*mb/str*	+	−
71.68	14.44	13.4	18.6
79.25	11.74	12.9	21.0
86.78	11.30	16.2	20.5

Avg. $d\sigma/d\omega$ = 11.99 mb/str ± 12.3%
$\int(d\sigma/d\omega)d\omega$ = 150.67 mb ± 12.3 %

$E_n = 5.23 \pm 0.05$ MeV
(n,n') to: 3.430 MeV Level
+ 3.490 MeV Level

θ_{cm}	$d\sigma/d\omega$	Δ (%)	
deg.	*mb/str*	+	−
71.81	12.46	16.1	25.0
79.39	13.30	13.7	20.2
86.93	12.82	15.8	23.1

Avg. $d\sigma/d\omega$ = 12.76 mb/str ± 13.9%
$\int(d\sigma/d\omega)d\omega$ = 160.36 mb ± 13.9 %

$E_n = 5.50 \pm 0.05$ MeV
(n,n') to: 1.434 MeV Level

θ_{cm}	$d\sigma/d\omega$	Δ (%)	
deg.	*mb/str*	+	−
48.45	14.91	19.9	13.3
56.06	11.28	14.6	14.2
63.65	10.89	27.7	25.8

$E_n = 5.50 \pm 0.05$ MeV
(n,n') to: 2.369 MeV Level

θ_{cm}	$d\sigma/d\omega$	Δ (%)	
deg.	*mb/str*	+	−
48.59	8.11	16.9	18.4
56.22	4.65	32.4	21.9
63.81	6.88	25.8	22.5

Avg. $d\sigma/d\omega$ = 6.57 mb/str ± 15.4%
$\int(d\sigma/d\omega)d\omega$ = 82.61 mb ± 15.4 %

$E_n = 5.50 \pm 0.05$ MeV
(n,n') to: 2.648 MeV Level
+ 2.766 MeV Level

θ_{cm}	$d\sigma/d\omega$	Δ (%)	
deg.	*mb/str*	+	−
48.67	11.04	16.2	26.8
56.29	8.51	13.6	21.4
63.90	8.83	25.4	31.9

Avg. $d\sigma/d\omega$ = 8.82 mb/str ± 13.7 %
$\int(d\sigma/d\omega)d\omega$ = 110.85 mb ± 13.7 %

$E_n = 5.50 \pm 0.05$ MeV
(n,n') to: 2.965 MeV Level

θ_{cm}	$d\sigma/d\omega$	Δ (%)	
deg.	*mb/str*	+	−
48.72	9.59	19.8	20.5
56.35	8.62	18.7	17.0
63.96	9.84	19.1	29.2

Avg. $d\sigma/d\omega$ = 9.14 mb/str ± 14.8 %
$\int(d\sigma/d\omega)d\omega$ = 114.82 mb ± 14.8 %

$E_n = 5.50 \pm 0.05$ MeV
(n,n') to: 3.112 MeV Level
+ 3.160 MeV Level

θ_{cm}	$d\sigma/d\omega$	Δ (%)	
deg.	*mb/str*	+	−
48.78	12.09	18.3	26.1
56.41	8.79	17.7	20.2
64.03	8.33	19.8	27.7

Avg. $d\sigma/d\omega$ = 8.96 mb/str ± 14.4 %
$\int(d\sigma/d\omega)d\omega$ = 112.60 mb ± 14.4 %

$E_n = 5.50 \pm 0.05$ MeV
(n,n') to: 3.430 MeV Level
+ 3.490 MeV Level

θ_{cm}	$d\sigma/d\omega$	Δ (%)	
deg.	*mb/str*	+	−
48.86	10.84	18.3	30.6
56.52	14.41	16.2	26.4
64.15	13.61	15.4	28.4

Avg. $d\sigma/d\omega$ = 11.91 mb/str ± 15.9 %
$\int(d\sigma/d\omega)d\omega$ = 149.61 mb ± 15.9 %

$E_n = 6.44 \pm 0.07$ MeV
Elastic Scattering

θ_{cm} deg.	$d\sigma/d\omega$ mb/str	Δ (%) +	Δ (%) −
15.29	2041.46	4.3	5.3
22.93	1460.73	4.1	4.2
28.01	1054.06	4.7	4.6
35.64	592.32	4.4	5.3
43.25	289.19	5.7	5.5
48.32	172.24	6.0	5.1
55.91	57.33	10.4	7.3
63.48	14.25	17.6	18.5
71.04	6.08	45.2	27.6
78.58	9.34	22.8	17.3
86.10	16.48	11.1	13.6
93.61	22.91	11.7	9.6
101.09	26.98	12.1	7.5
108.56	27.26	11.5	9.3
120.46	24.58	8.7	7.7
127.88	19.43	11.5	9.8
135.29	12.58	14.5	14.6

$\int(d\sigma/d\omega)d\omega$ =2179.94 mb ± 7.2 %
Wick's Limit =2401.27 mb ± 7.3 %
σ_T = 3.56 b ± 1.0 %

Legendre Fit, Order = 8

k	a_k	Δ(%)
0	346.94800	1.9
1	278.89722	2.1
2	217.43750	2.3
3	155.66310	2.6
4	90.21782	3.6
5	42.95523	5.7
6	18.38136	9.4
7	5.85265	18.2
8	1.31388	49.0

$E_n = 6.44 \pm 0.07$ MeV
(n,n') to: 1.434 MeV Level

θ_{cm} deg.	$d\sigma/d\omega$ mb/str	Δ (%) +	Δ (%) −
28.09	17.33	19.8	31.8
35.72	14.10	15.9	23.3
43.35	13.92	12.1	15.7
48.43	13.23	15.0	14.0
56.03	11.71	12.9	15.1
63.62	9.83	10.9	12.2
71.18	8.31	13.4	6.9
78.73	8.01	15.9	11.6
86.25	7.18	11.6	16.7
93.75	8.07	10.9	11.6
101.24	7.56	15.3	14.6
108.70	8.29	14.0	12.2
120.60	11.50	13.1	14.4
128.01	11.18	13.2	11.3
135.40	11.95	14.1	10.9

$\int(d\sigma/d\omega)d\omega$ = 137.30 mb ± 8.1 %

Legendre Fit, Order = 2

k	a_k	Δ(%)
0	21.85197	4.0
1	0.48316	110.7
2	2.69826	17.2

$E_n = 6.44 \pm 0.07$ MeV
(n,n') to: 2.369 MeV Level

$\theta_{c.m.}$ deg.	$d\sigma/d\omega$ mb/str	Δ (%) +	Δ (%) −
28.15	8.17	19.1	26.3
35.81	7.44	25.3	33.0
43.44	6.26	20.8	26.3
48.53	4.56	18.2	24.5
56.15	4.96	12.0	21.8
63.74	4.97	18.1	24.1
71.32	4.91	17.7	19.0
78.87	4.12	18.5	13.2
86.40	4.79	16.1	20.9
93.90	4.49	23.0	22.5
101.38	5.60	19.1	20.9
108.84	5.35	21.6	26.2
120.72	5.21	15.1	15.6
128.12	4.45	26.1	24.0
135.50	4.60	14.2	22.5

Avg. $d\sigma/d\omega$ = 4.86 mb/str ± 9.6 %
$\int(d\sigma/d\omega)d\omega$ = 61.02 mb ± 9.6 %

$E_n = 7.03 \pm 0.06$ MeV
(n,n') to: 1.434 MeV Level

θ_{cm} deg.	$d\sigma/d\omega$ mb/str	Δ (%) +	Δ (%) −
71.17	6.71	10.0	12.6
78.71	5.50	17.7	13.3
86.23	5.34	15.1	12.6

$E_n = 7.03 \pm 0.06$ MeV
(n,n') to: 2.369 MeV Level

θ_{cm} deg.	$d\sigma/d\omega$ mb/str	Δ (%) +	Δ (%) −
71.28	3.09	11.9	20.5
78.83	2.77	17.1	29.4
86.36	2.96	14.3	23.6

Avg. $d\sigma/d\omega$ = 2.90 mb/str ± 13.8 %
$\int(d\sigma/d\omega)d\omega$ = 36.42 mb ± 13.8 %

$E_n = 7.54 \pm 0.05$ MeV
Elastic Scattering

θ_{cm} deg.	$d\sigma/d\omega$ mb/str	Δ (%) +	Δ (%) −
15.29	2059.81	4.3	4.6
22.92	1369.98	4.3	4.9
28.01	930.04	5.2	6.1
35.64	480.46	5.0	5.5
43.25	201.13	5.8	5.6
48.32	103.89	10.1	8.1
48.32	111.34	8.3	5.5
55.91	30.63	14.5	11.6
55.91	26.70	15.2	12.6
63.48	6.18	28.3	32.0
63.48	8.57	22.7	25.8
71.04	5.07	31.6	31.8
78.58	8.88	14.8	17.4
86.10	11.87	12.8	10.3
93.60	15.05	9.8	12.6
101.09	17.41	13.9	8.1
108.55	18.14	8.8	9.6
120.46	16.44	13.5	10.1
127.88	10.53	11.0	14.4
135.29	6.33	18.1	19.7

$\int(d\sigma/d\omega)d\omega$ = 1914.77 mb ± 7.3 %
Wick's Limit = 2474.68 mb ± 7.3 %
σ_T = 3.34 b ± 1.0 %

Legendre Fit, Order = 8

k	a_k	Δ(%)
0	304.74561	2.1
1	255.33163	2.3
2	204.707[illegible]	2.4
3	151.2162[illegible]	2.6
4	95.13348	3.2
5	50.30403	4.3
6	23.83644	6.0
7	8.42546	9.9
8	2.00243	24.2

E_n = 7.54 ± 0.06 MeV
(n,n') to: 1.434 MeV Level

θ_{cm}	dσ/dω	Δ (%)	
deg.	*mb/str*	+	−
35.71	9.38	21.7	27.9
43.33	9.34	19.0	17.8
48.41	7.89	25.6	15.7
48.41	7.93	20.1	13.5
56.01	6.65	17.1	11.5
56.01	8.24	9.8	9.8
63.59	7.45	17.5	11.4
63.59	6.48	14.4	11.7
71.16	5.75	19.1	11.2
78.70	6.00	23.3	14.4
86.22	5.04	18.2	15.3
93.73	4.66	16.0	19.2
101.21	4.70	14.5	15.3
108.67	4.62	15.3	18.5
120.57	7.71	13.2	20.2
127.98	8.87	10.4	12.6
135.38	9.77	8.8	11.7

∫(dσ/dω)dω = 96.47 mb ± 8.0 %

Legendre Fit, Order = 2

k	a_k	Δ(%)
0	15.35375	3.9
1	−0.00133	100.0
2	2.33334	15.3

E_n = 7.54 ± 0.06 MeV
(n,n') to: 2.369 MeV Level

θ_{cm}	dσ/dω	Δ (%)	
deg.	*mb/str*	+	−
43.41	3.11	26.8	31.5
48.49	3.22	27.0	36.1
48.49	3.03	24.8	35.2
56.10	2.53	23.9	24.5
56.10	2.23	33.0	30.7
63.69	2.90	32.8	26.3
63.69	2.30	39.0	24.6
71.26	2.70	25.9	36.9
78.80	3.26	26.9	17.4
86.33	2.59	21.2	27.0
93.84	2.38	22.4	28.9
101.32	2.20	20.8	33.1
108.77	2.29	20.9	31.0
120.67	1.98	20.2	31.9
128.07	1.83	22.3	26.3
135.46	1.89	20.8	37.5

Avg. dσ/dω = 2.29 mb/str ± 10.2%
∫(dσ/dω)dω = 28.83 mb ± 10.2 %

E_n = 8.04 ± 0.05 MeV
(n,n') to: 1.434 MeV Level

θ_{cm}	dσ/dω	Δ (%)	
deg.	*mb/str*	+	−
71.15	4.42	23.4	17.0
78.69	4.72	13.4	20.6
86.22	4.37	20.1	24.6

E_n = 8.04 ± 0.05 MeV
(n n') to: 2.369 MeV Level

θ_{cm}	dσ/dω	Δ (%)	
deg.	*mb/str*	+	−
71.24	1.59	42.9	28.6
78.79	2.15	24.4	31.3
86.32	0.95	78.8	29.6

Avg. dσ/dω = 1.61 mb/str ± 26.2%
∫(dσ/dω)dω = 20.24 mb ± 26.2 %

$E_n = 8.56 \pm 0.05$ MeV
Elastic Scattering

θ_{cm} *deg.*	$d\sigma/d\omega$ *mb/str*	Δ (%) +	Δ (%) −
15.29	2066.95	5.6	7.1
22.93	1342.76	5.1	8.3
28.01	862.89	5.6	6.8
35.64	399.88	5.5	7.9
43.25	160.22	7.1	6.7
48.32	78.89	9.1	10.1
55.91	19.83	15.4	18.5
63.48	5.50	30.1	32.4
71.04	7.61	28.2	28.6
78.58	8.18	15.9	23.6
86.10	10.37	17.7	15.6
93.60	15.02	10.2	14.3
101.09	17.71	8.2	13.8
108.55	18.08	9.1	10.7
120.46	15.22	11.4	13.3
127.88	8.59	17.5	18.7
135.29	5.44	21.3	24.1

$\int(d\sigma/d\omega)d\omega$ = 1790.89 mb ± 7.5 %
Wick's Limit = 2514.80 mb ± 7.3 %
σ_T = 3.16 b ± 1.0 %

Legendre Fit, Order = 9

k	a_k	Δ(%)
0	285.02979	2.7
1	240.45734	2.9
2	196.80482	3.1
3	150.06050	3.4
4	99.47911	4.1
5	56.69565	5.5
6	30.02299	7.4
7	12.83146	11.8
8	4.16914	22.0
9	1.01623	49.3

$E_n = 8.56 \pm 0.05$ MeV
(n,n') to: 1.434 MeV Level

θ_{cm} *deg.*	$d\sigma/d\omega$ *mb/str*	Δ (%) +	Δ (%) −
35.70	8.68	39.3	29.6
43.32	8.93	12.9	23.5
48.39	5.80	20.7	19.5
55.99	5.29	25.4	17.9
63.58	5.04	19.0	12.2
71.14	6.23	22.9	15.6
78.68	5.56	11.5	12.8
86.21	5.05	16.1	24.2
93.71	4.46	23.5	25.6
101.19	3.45	24.8	18.3
108.65	4.43	12.3	21.6
120.55	5.37	12.2	16.2
127.97	4.90	21.8	23.7
135.36	5.20	18.3	16.7

$\int(d\sigma/d\omega)d\omega$ = 69.10 mb ± 8.9 %

Legendre Fit, Order = 2

k	a_k	Δ(%)
0	10.99744	5.5
1	0.79444	47.9
2	0.71028	47.5

$E_n = 8.56 \pm 0.05$ MeV
(n,n') to: 2.369 MeV Level

θ_{cm} *deg.*	$d\sigma/d\omega$ *mb/str*	Δ (%) +	Δ (%) −
43.38	3.59	21.6	35.7
48.46	1.61	38.5	38.5
63.66	1.49	40.2	37.2
71.22	1.25	45.8	41.8
78.77	1.98	28.7	33.1
86.29	1.62	22.9	34.0
93.80	1.72	33.7	31.9
101.28	1.71	27.7	35.3
108.74	1.49	32.4	34.7
120.64	1.44	35.1	38.4
128.04	1.23	34.9	40.3
135.43	1.37	34.6	25.7

Avg. $d\sigma/d\omega$ = 1.53 mb/str ± 13.1 %
$\int(d\sigma/d\omega)d\omega$ = 19.27 mb ± 13.1 %

^{52}Cr CROSS SECTIONS

$E_n = 6.44 \pm 0.07$ MeV
Elastic Scattering

θ_{cm} *deg.*	$d\sigma/d\omega$ *mb/str*	Δ (%) +	Δ (%) −
15.29	1954.92	4.4	5.7
22.93	1440.22	4.4	6.1
28.01	1147.87	4.1	3.9
35.64	675.50	4.5	4.8
43.25	329.01	5.8	5.1
48.32	156.77	6.4	5.7
55.91	46.71	16.4	12.0
63.48	10.45	42.8	22.1
71.04	5.85	48.8	34.3
78.58	9.77	19.7	19.6
86.10	15.82	11.9	12.2
93.61	22.42	15.0	15.0
101.09	27.78	7.7	9.7
108.56	27.90	6.6	7.8
120.46	24.75	7.5	8.2
127.89	17.21	9.2	9.9
135.29	15.01	9.8	14.6

$\int(d\sigma/d\omega)d\omega$ = 2230.36 mb ± 7.3 %
Wick's Limit = 2401.17 mb ± 7.3 %
σ_T = 3.56 b ± 1.0 %

Legendre Fit, Order = 9

k	a_k	Δ(%)
0	354.97266	1.9
1	285.54443	2.2
2	223.00180	2.4
3	158.17705	2.8
4	89.73320	4.1
5	40.09595	7.5
6	14.05306	16.9
7	2.07775	83.5
8	−1.33218	82.2
9	−1.07083	55.3

$E_n = 6.44 \pm 0.07$ MeV
(n,n′) to: 1.434 MeV Level

θ_{cm} *deg.*	$d\sigma/d\omega$ *mb/str*	Δ (%) +	Δ (%) −
35.72	7.64	75.4	22.8
43.35	14.01	12.8	20.4
48.43	14.63	18.2	18.2
56.03	11.79	18.6	13.9
63.62	10.58	13.9	15.3
71.18	10.35	13.7	11.8
78.73	8.69	17.9	14.2
86.25	8.35	22.2	10.7
93.76	8.93	18.2	14.9
101.24	7.82	14.7	18.0
108.70	9.69	13.8	7.7
120.60	11.98	11.0	12.4
128.00	12.95	8.6	18.7
135.40	13.49	11.9	19.9

$\int(d\sigma/d\omega)d\omega$ = 146.51 mb ± 8.5 %

Legendre Fit, Order = 2

k	a_k	Δ(%)
0	23.31750	4.8
1	−0.09398	713.7
2	2.33285	26.5

$E_n = 6.44 \pm 0.07$ MeV
(n,n′) to: 2.369 MeV Level

θ_{cm} *deg.*	$d\sigma/d\omega$ *mb/str*	Δ (%) +	Δ (%) −
48.53	5.04	23.0	26.9
56.15	3.43	55.4	19.4
63.74	5.46	15.8	21.4
71.32	5.64	25.1	18.8
78.87	4.64	23.5	18.9
86.30	5.14	21.6	23.7
93.90	6.21	16.3	16.6
101.38	4.90	16.9	14.3
108.84	3.73	16.7	16.8
120.72	5.01	13.3	24.6
128.12	3.96	21.7	28.1
135.50	4.23	11.2	19.1

Avg. $d\sigma/d\omega$ = 4.56 mb/str ± 9.6 %
$\int(d\sigma/d\omega)d\omega$ = 57.35 mb ± 9.6 %

$E_n = 7.03 \pm 0.06$ MeV
(n,n') to: 1.434 MeV Level

θ_{cm}	$d\sigma/d\omega$	Δ (%)	
deg.	*mb/str*	+	−
71.17	7.43	7.3	10.5
78.71	6.07	7.2	16.4
86.24	5.52	11.4	12.9

$E_n = 7.03 \pm 0.06$ MeV
(n,n') to: 2.369 MeV Level

θ_{cm}	$d\sigma/d\omega$	Δ (%)	
deg.	*mb/str*	+	−
71.28	3.37	12.6	16.7
78.83	3.21	10.6	14.0
86.36	3.36	13.0	17.2

Avg. $d\sigma/d\omega$ = 3.27 mb/str ± 11.0%
$\int(d\sigma/d\omega)d\omega$ = 41.10 mb ± 11.0 %

$E_n = 7.54 \pm 0.06$ MeV
Elastic Scattering

θ_{cm}	$d\sigma/d\omega$	Δ (%)	
deg.	*mb/str*	+	−
15.29	1974.98	4.8	7.5
22.93	1349.41	5.1	6.6
28.01	911.55	4.8	7.4
35.64	482.87	5.7	9.6
43.25	196.85	6.9	6.6
48.32	109.96	12.0	4.7
55.91	35.54	14.3	11.4
63.48	8.86	19.2	32.9
71.04	6.03	21.7	27.2
78.58	8.21	13.5	20.7
86.10	10.52	11.4	14.8
93.60	14.96	12.2	14.2
101.09	18.02	8.1	8.0
108.55	20.77	7.0	10.7
120.46	15.49	10.4	13.1
127.88	10.47	10.8	14.2
135.29	6.54	17.0	17.3

$\int(d\sigma/d\omega)d\omega$ = 1888.44 mb ± 7.4 %
Wick's Limit = 2474.58 mb ± 7.3 %
σ_T = 3.34 b ± 1.0 %

Legendre Fit, Order = 10

k	a_k	Δ(%)
0	300.55518	2.5
1	251.15988	2.8
2	201.86864	3.0
3	150.44354	3.3
4	95.93333	4.3
5	53.04265	6.4
6	27.62170	10.1
7	12.18252	17.7
8	4.47375	33.4
9	1.66845	54.5
10	0.58864	81.1

$E_n = 7.54 \pm 0.06$ MeV
(n,n′) to: 1.434 MeV Level

θ_{cm} deg.	$d\sigma/d\omega$ mb/str	Δ (%) +	Δ (%) −
35.71	11.31	17.9	19.3
43.33	9.51	14.0	23.1
48.41	9.44	16.6	17.3
56.01	8.00	9.8	10.3
63.59	7.48	12.7	11.7
71.16	7.35	12.8	12.2
78.70	7.08	9.4	14.1
86.22	6.15	15.1	12.5
93.73	5.27	11.3	23.2
101.21	5.70	12.0	23.0
108.67	6.25	13.8	25.5
120.57	9.01	26.8	15.5
127.98	15.54	5.9	10.5
135.38	16.45	7.2	11.4

$\int(d\sigma/d\omega)d\omega =$ 131.54 mb $\pm$ 8.0 %

Legendre Fit, Order = 2

k	a_k	Δ(%)
0	20.93494	3.9
1	−2.15703	22.8
2	3.63094	12.1

$E_n = 7.54 \pm 0.06$ MeV
(n,n′) to: 2.369 MeV Level

θ_{cm} deg.	$d\sigma/d\omega$ mb/str	Δ (%) +	Δ (%) −
43.40	3.74	31.9	36.0
48.49	2.50	46.7	30.1
56.10	2.73	15.2	26.3
63.69	3.22	24.6	20.3
71.26	3.41	28.4	27.4
78.81	2.24	40.7	23.6
86.33	2.97	15.0	17.1
93.84	2.59	13.1	26.0
101.32	2.38	14.5	25.7
108.78	2.93	16.0	25.4
120.67	2.02	19.4	25.7
128.07	2.22	16.8	29.0
135.46	1.78	14.8	25.7

Avg. $d\sigma/d\omega =$ 2.29 mb/str $\pm$ 10.1 %
$\int(d\sigma/d\omega)d\omega =$ 28.83 mb $\pm$ 10.1 %

$E_n = 8.04 \pm 0.05$ MeV
(n,n′) to: 1.434 MeV Level

θ_{cm} deg.	$d\sigma/d\omega$ mb/str	Δ (%) +	Δ (%) −
71.15	7.36	9.7	14.3
78.69	6.68	14.2	17.4
86.22	5.33	11.0	15.0

$E_n = 8.04 \pm 0.05$ MeV
(n,n′) to: 2.369 MeV Level

θ_{cm} deg.	$d\sigma/d\omega$ mb/str	Δ (%) +	Δ (%) −
71.24	2.83	17.2	34.7
78.79	3.07	19.9	21.1
86.32	2.30	29.9	28.4

Avg. $d\sigma/d\omega =$ 2.73 mb/str $\pm$ 17.3 %
$\int(d\sigma/d\omega)d\omega =$ 34.36 mb $\pm$ 17.3 %

$E_n = 8.56 \pm 0.05$ MeV
Elastic Scattering

θ_{cm} *deg.*	$d\sigma/d\omega$ *mb/str*	Δ (%) +	Δ (%) −
15.29	2050.69	5.4	7.9
22.92	1240.76	5.7	5.3
28.01	736.22	6.9	4.1
35.63	361.06	6.7	5.2
43.25	143.86	7.9	7.5
48.32	100.08	6.7	7.9
55.91	22.58	13.7	12.8
63.48	8.93	12.5	22.7
71.04	6.79	21.8	32.8
78.58	8.58	14.3	17.4
86.10	9.86	12.4	17.0
93.60	12.55	13.1	16.4
93.61	12.74	11.0	17.1
101.09	15.87	9.2	15.1
101.09	13.51	18.6	20.5
108.55	18.11	9.3	19.7
108.55	16.23	10.8	15.8
120.46	15.80	8.7	13.7
127.88	10.11	14.4	15.8
135.29	5.27	17.6	23.9

$\int(d\sigma/d\omega)d\omega = 1687.03\,\text{mb} \pm 7.4\ \%$
Wick's Limit $= 2514.69\,\text{mb} \pm 7.3\ \%$
$\sigma_T = 3.16\,\text{b} \pm 1.0\ \%$

Legendre Fit, Order = 10

k	a_k	Δ(%)
0	268.49927	2.5
1	226.42068	2.8
2	185.15302	3.0
3	142.47368	3.4
4	95.47168	4.2
5	57.52827	5.8
6	33.21892	7.8
7	16.75014	11.6
8	7.63199	17.0
9	3.47761	22.4
10	1.08875	36.1

$E_n = 8.56 \pm 0.05$ MeV
(n,n') to: 1.434 MeV Level

θ_{cm} *deg.*	$d\sigma/d\omega$ *mb/str*	Δ (%) +	Δ (%) −
35.70	8.95	15.3	29.1
43.32	9.85	12.7	22.7
48.39	6.44	15.0	17.7
55.99	6.65	14.1	11.2
63.58	6.23	9.2	15.3
71.14	5.98	19.7	18.8
78.68	6.30	13.9	21.6
86.20	5.02	15.3	12.5
93.71	5.50	18.1	33.6
93.71	5.31	20.2	24.4
101.19	4.78	33.8	36.2
101.19	3.81	33.6	29.9
108.65	6.13	19.8	33.2
108.65	5.94	14.1	30.1
120.56	6.63	25.9	13.6
127.97	9.54	11.7	25.5
135.36	7.93	13.3	28.6

$\int(d\sigma/d\omega)d\omega = 86.76\,\text{mb} \pm 8.8\ \%$

Legendre Fit, Order = 2

k	a_k	Δ(%)
0	13.80893	5.4
1	−0.01754	2601.6
2	1.37699	28.3